

Supporting Information

Four Novel Aporphine- and Proaporphine-Clerodane Hybrids from the Barks of Taiwanese *Polyalthia longifolia* var. *pendula* with Strong Anti-DENV2 Activity

I-Wen Lo ¹, Geng-You Liao ², Jin-Ching Lee ³, Chi-I Chang ⁴, Yang-Chang Wu ^{5,6}, Yen-Yu Chen ⁷, Shang-Pin Liu ⁸, Huey-Jen Su ⁹, Chih-I Liu ⁹, Chia-Yi Kuo ¹⁰, Zheng-Yu Lin ¹⁰, Tsung-Lin Li ^{1,*}, Yun-Sheng Lin ^{10,*} and Chia-Ching Liaw ^{11,12,*}

¹ Genomics Research Center, Academia Sinica, Taipei 115201, Taiwan.

² Institute of Physiology, School of Medicine, National Yang Ming Chiao Tung University, Taipei 112304, Taiwan

³ Department of Marine Biotechnology and Resources, National Sun Yat-sen University, Kaohsiung 804201, Taiwan.

⁴ Department of Biological Science and Technology, National Pingtung University of Science and Technology, Pingtung 912301, Taiwan

⁵ Chinese Medicine Research and Development Center, China Medical University Hospital, Taichung 404332, Taiwan

⁶ Graduate Institute of Integrated Medicine, College of Chinese Medicine, China Medical University, Taichung 404333, Taiwan.

⁷ Department of Education and Research, Taipei City Hospital, Taipei 103212, Taiwan

⁸ Bachelor of Program in Scientific Agriculture, National Pingtung University of Science and Technology, Pingtung 912301, Taiwan.

⁹ Department of Nursing, Meoho University, Pingtung 912009, Taiwan.

¹⁰ Department of Biological Science and Technology, Meoho University, Pingtung 912009, Taiwan.

¹¹ Division of Chinese Material Medica Development, National Research Institute of Chinese Medicine,

Taipei 112026, Taiwan

¹² Department of Biochemical Science and Technology, National Chiayi University, Chiayi 600355, Taiwan

* Corresponding author: Chia-Ching Liaw, National Research Institute of Chinese Medicine, Taipei 112026, Taiwan. E-mail address: liawcc@nricm.edu.tw (C.C. Liaw). Tsung-Lin Li, Genomics Research Center, Academia Sinica, Taipei 115201, Taiwan. E-mail address: tlli@gate.sinica.edu.tw (T.L. Li). Yun-Sheng Lin, Department of Biological Science and Technology, Meiho University, Pingtung 912009, Taiwan. E-mail address: x00010106@meiho.edu.tw (Y.S. Lin).

Figure S1. The $\omega_{16\text{-N,C-16,C-13,C-12}}$ torsional angles of *cis*-**1** (A), *trans*-**1** (B), *cis*-**3m-16R** (C), and *trans*-**3m-16R** (D).

Figure S2. Proposed biosynthetic pathways of **1-4**.

Figure S3. Protein sequence alignments of various flavivirus NS2B-NS3 proteases including DENV serotypes **1-4**, Zika virus, West Nile virus (WNV), and Murray Valley encephalitis virus (MVEV).

Figure S4. Protein crystal structures of NS2B-NS3 proteases in DENV serotypes 1-4.

Figure S5. AutoDock 4.2 of binding simulation between DENV2 NS2B-NS3 protease and **1-4**.

Table S1. Crystal data and structure refinement for **1**.

Table S2. Atomic coordinates and equivalent isotropic displacement parameters for **1**. U(eq) is defined as one third of the trace of the orthogonalized U tensor.

Table S3. The Predicted Binding Affinity and RMSD bounds of **1-4**.

Table S4. Python Shell Information of **1-4** in Different Models.

References

Spectra of compounds **1-4**

Figure PA-1. ESI-MS spectrum of polyalongarin A (**1**)

Figure PA-2. HR-ESI-MS spectrum of polyalongarin A (**1**)

Figure PA-3. UV spectrum of polyalongarin A (**1**)

Figure PA-4. IR spectrum of polyalongarin A (**1**)

Figure PA-5. CD spectrum of polyalongarin A (**1**)

Figure PA-6. ^1H -NMR spectrum of polyalongarin A (**1**) in CDCl_3 (500 MHz)

Figure PA-7. ^{13}C -NMR spectrum of polyalongarin A (**1**) in CDCl_3 (125 MHz)

Figure PA-8. DEPT-135 and DEPT-90 spectra of polyalongarin A (**1**)

Figure PA-9. HMQC spectrum of polyalongarin A (**1**)

Figure PA-10. COSY spectrum of polyalongarin A (**1**)

Figure PA-11. HMBC spectrum of polyalongarin A (**1**)

Figure PA-12. NOESY spectrum of polyalongarin A (**1**)

Figure PB-1. ESI-MS spectrum of polyalongarin B (**2**)

Figure PB-2. HR-ESI-MS spectrum of polyalongarin B (**2**)

Figure PB-3. UV spectrum of polyalongarin B (**2**)

Figure PB-4. IR spectrum of polyalongarin B (**2**)

Figure PB-5. CD spectrum of polyalongarin B (**2**)

Figure PB-6. ^1H -NMR spectrum of polyalongarin B (**2**) in CDCl_3 (500 MHz)

Figure PB-7. ^{13}C -NMR spectrum of polyalongarin B (2) in CDCl_3 (125 MHz)

Figure PB-8. DEPT-135 and DEPT-90 spectra of polyalongarin B (2)

Figure PB-9. HMQC spectrum of polyalongarin B (2)

Figure PB-10. COSY spectrum of polyalongarin B (2)

Figure PB-11. HMBC spectrum of polyalongarin B (2)

Figure PB-12. NOESY spectrum of polyalongarin B (2)

Figure PC-1. ESI-MS spectrum of polyalongarin C (3)

Figure PC-2. HR-ESI-MS spectrum of polyalongarin C (3)

Figure PC-3. UV spectrum of polyalongarin C (3)

Figure PC-4. IR spectrum of polyalongarin C (3)

Figure PC-5. CD spectrum of polyalongarin C (3)

Figure PC-6. ^1H -NMR spectrum of polyalongarin C (3) in CDCl_3 (500 MHz)

Figure PC-7. ^{13}C -NMR spectrum of polyalongarin C (3) in CDCl_3 (125 MHz)

Figure PC-8. DEPT-135 and DEPT-90 spectra of polyalongarin C (3)

Figure PC-9. HMQC spectrum of polyalongarin C (3)

Figure PC-10. COSY spectrum of polyalongarin C (3)

Figure PC-11. HMBC spectrum of polyalongarin C (3)

Figure PC-12. NOESY spectrum of polyalongarin C (3)

Figure PD-1. ESI-MS spectrum of polyalongarin D (4)

Figure PD-2. HR-ESI-MS spectrum of polyalongarin D (4)

Figure PD-3. UV spectrum of polyalongarin D (4)

Figure PD-4. IR spectrum of polyalongarin D (4)

Figure PD-5. CD spectrum of polyalongarin D (4)

Figure PD-6. ^1H -NMR spectrum of polyalongarin D (4) in CDCl_3 (500 MHz)

Figure PD-7. ^{13}C -NMR spectrum of polyalongarin D (4) in CDCl_3 (125 MHz)

Figure PD-8. DEPT-135 and DEPT-90 spectra of polyalongarin D (4)

Figure PD-9. HMQC spectrum of polyalongarin D (4)

Figure PD-10. COSY spectrum of polyalongarin D (4)

Figure PD-11. HMBC spectrum of polyalongarin D (4)

Figure PD-12. NOESY spectrum of polyalongarin D (4)

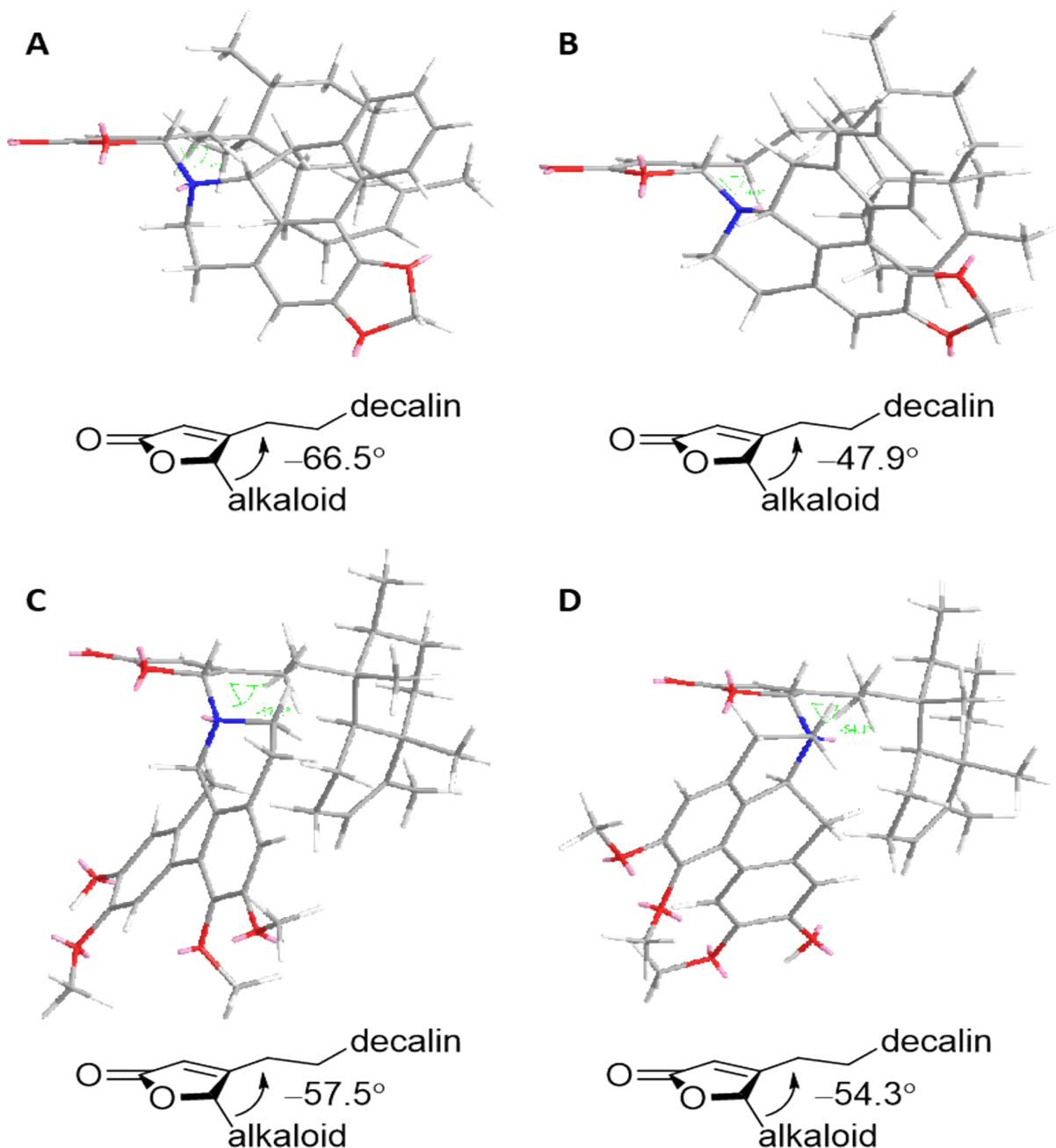


Figure S1. The $\omega_{16-N,C-16,C-13,C-12}$ torsional angles of *cis*-**1** (A), *trans*-**1** (B), *cis*-**3m-16R** (C), and *trans*-**3m-16R** (D). The dihedral angles are -66.5° , -47.9° , -57.5° , and -54.3° , respectively calculated after MMFF94 minimization by Chem3D 16.0 with the β -oriented H-16. The negative $\omega_{16-N,C-16,C-13,C-12}$ torsional angles are counterclockwise in both *cis*- and *trans*-form of **3m-16R** (*cis*- and *trans*-form here are the configurations of H-7' and the lone pair on 16-N atom), suggesting that the orientation of the lone pair on N atom does not alter the exciton-coupled system in a manner akin to *cis*-**1** or *trans*-**1**. The dihedral angle between aprophine and ethyl-tetramethyl-octahydronaphthalene (decalin) of **3m-16R** remains the same, while the helical conformation of the five-membered γ -lactone ring and aprophine is altered to *P*-configuration by β -directed H-7'.

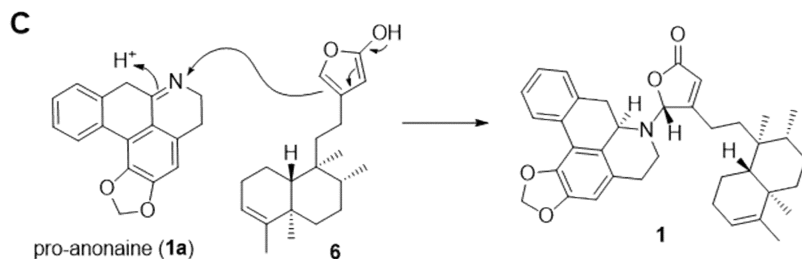
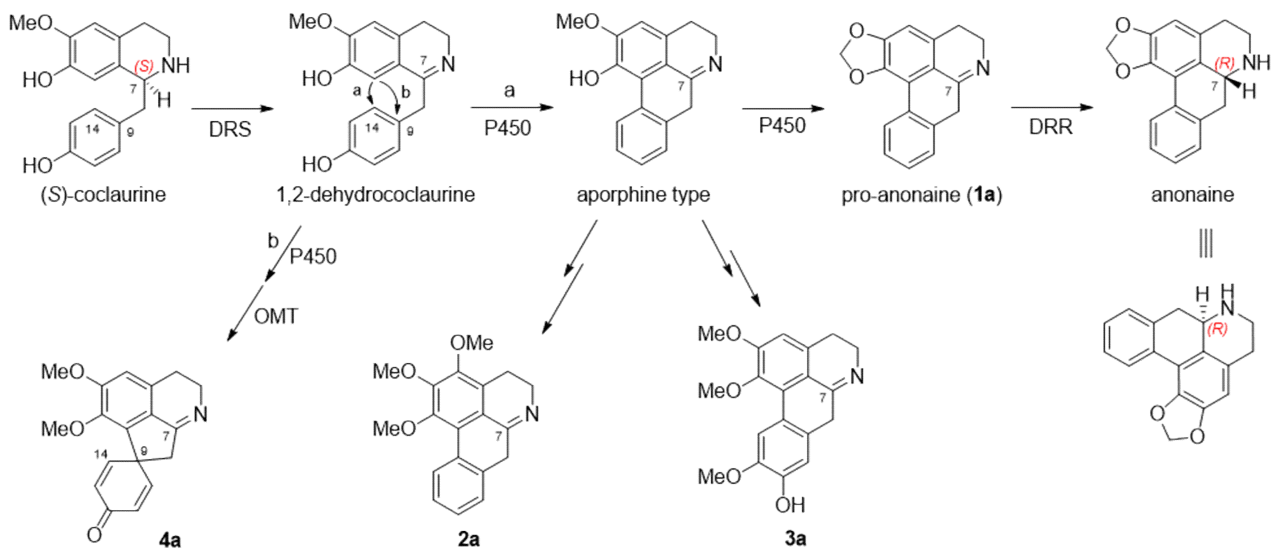
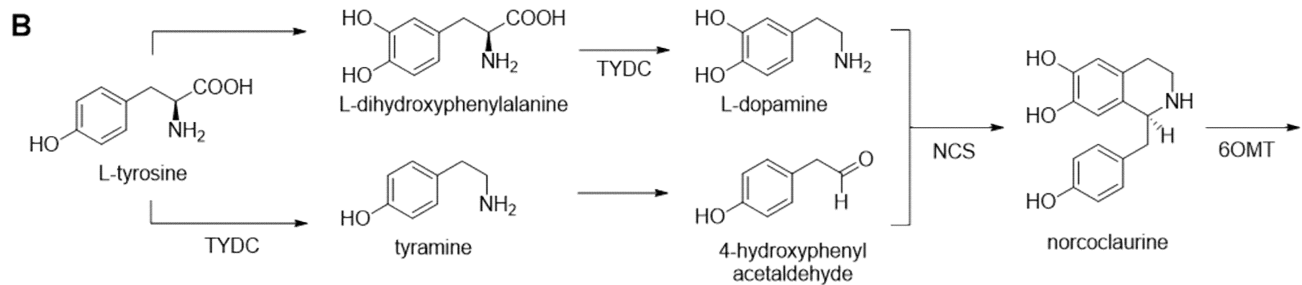
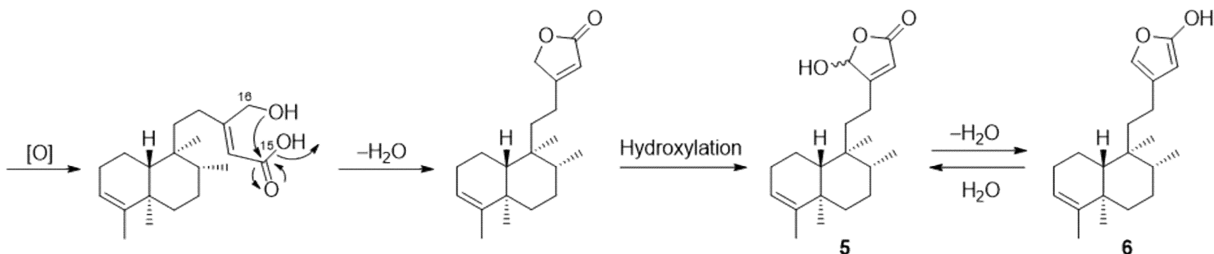
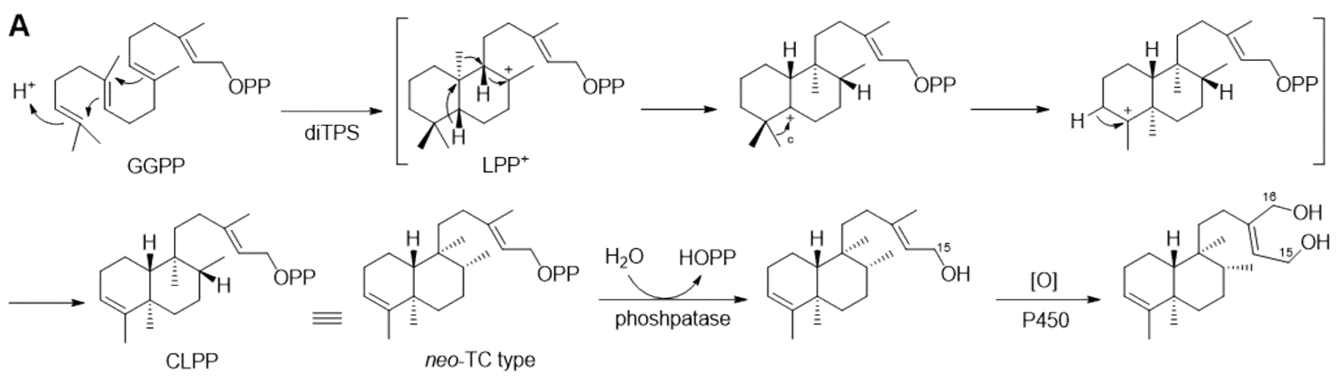
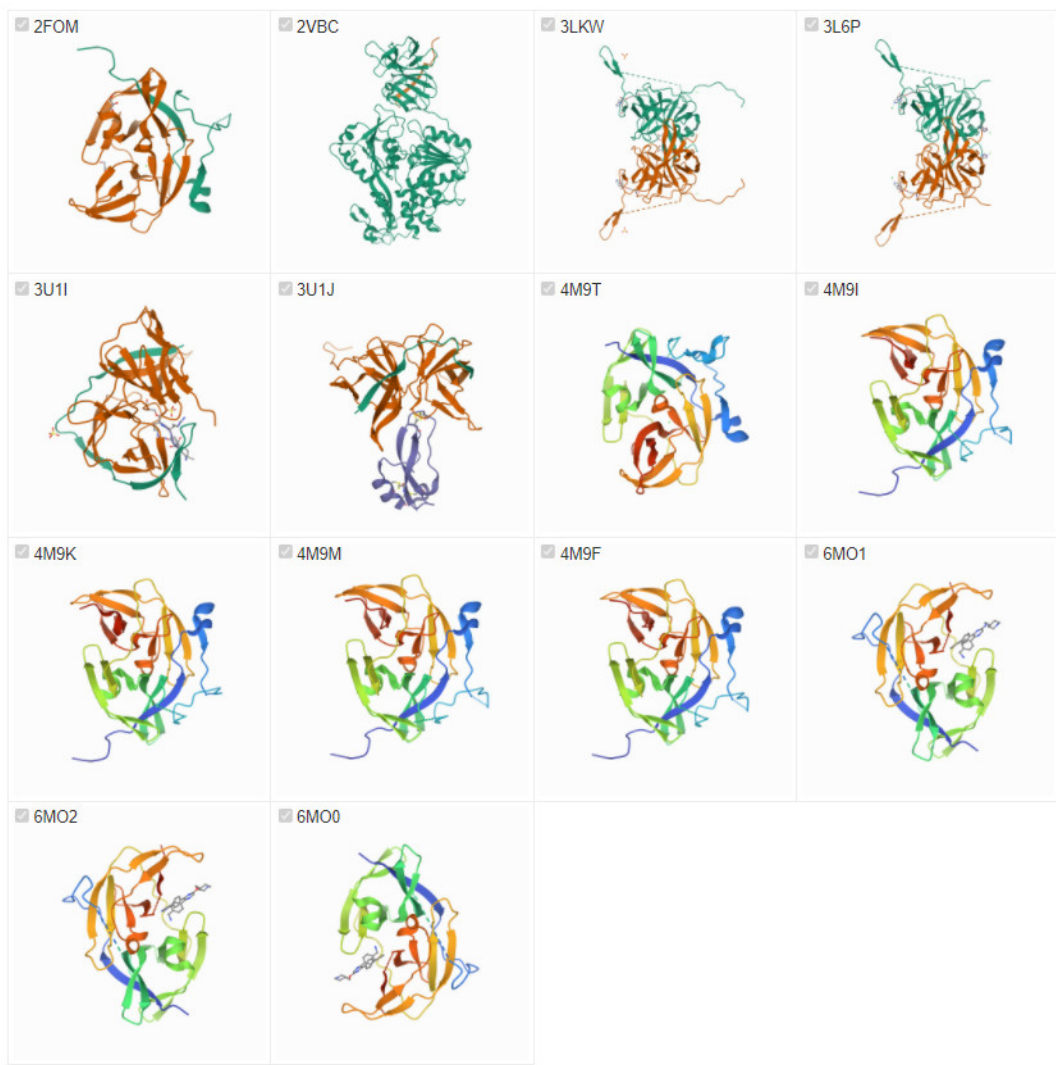


Figure S2. Proposed biosynthetic pathways of **1-4**.¹ (A) Formation of clerodane-type diterpenoids: The common diterpenoid precursor (*E,E,E*)-geranylgeranyl pyrophosphate (GGPP) is cyclized by a class II diterpene synthetase (diTPS), which protonates the terminal C=C bond of GGPP and cyclizes to the bicyclic (*trans*-decalin) intermediate, labda-13*E*-en-8-yl⁺ pyrophosphate (LPP⁺), via sequential anti addition from the internal double bonds of GGPP. Next, a cascade of 1,2-hydride and methyl shifts produce clerodiienyl pyrophosphate (CLPP), and then phosphatase removes the diphosphate, leading a fully rearranged clerodane type skeleton backbone. After cytochrome P450 monooxygenase (P450) oxidation, C-16 is hydroxylated and 15,16-dihydroxyl clerodane is formed. Further oxidation at C-15 to form a carboxylic acid. The final clerodane-type diterpenoids, 16-hydroxycleroda-3,13(14)Z-dien-15,16-olide (**5**), is given by the following dehydration, hydroxylation, and dehydration. Further dehydration affords the 15-hydroxyfuran-containg clerodane (**6**). (B) Formation of aporphine/proaporphine alkaloids: L-tyrosine is hydroxylated and decarboxylated by DOPA decarboxylase (TYDC) to form L-dopamine and 4-hydroxyphenyl acetaldehyde. These two moieties are condensed to be a benzylisoquinoline-type alkaloid, norcoclaurine, by norcoclaurine synthase (NCS). Norcoclaurine is further methylated by norcoclaurine 6-*O*-methyltransferase (6OMT) to form (*S*)-coclaurine, which is the common precursor of aporphine and proaporphine alkaloids. After the oxidation of (*S*)-coclaurine to 1,2-dehydrococlaurine by 1,2-dehydroreticuline synthase (DRS), following the oxidative coupling aromatization at C-14 (pathway a) produces dehydrogenated aporphines **1a-3a** while the dienone-phenol rearrangement at C-9 (pathway b) gives proaporphine **4a**. Then, a series of P450 oxidation, *O*-methylation, and/or hydroxylation are occurred, and these pro-chiral compounds are reduced by 1,2-dehydroreticuline reductase (DRR), leading the production of 7*R* alkaloids, such as anonaine. (C) These clerodane-alkaloid hybrids are assumed to be made from DRR homologues by electron transfer-induced nucleophilic addition reaction, for instance, polyalongarin A (**1**) is a merged by anonaine (**1a**) and **6**.





| PDB ID | Structure Title |
|----------------------|--|
| 2FOM | Dengue Virus 2 NS2B/NS3 Protease |
| 2VBC | Crystal structure of the NS3 protease-helicase from Dengue virus 4 |
| 3LKW | Crystal Structure of Dengue Virus 1 NS2B/NS3 protease active site mutant |
| 3L6P | Crystal Structure of Dengue Virus 1 NS2B/NS3 protease |
| 3U1I | Dengue virus 3 protease covalently bound to a peptide |
| 3U1J | Aprotinin bound to Dengue virus 3 protease |
| 4M9T | NS2B-NS3 protease from dengue virus 2 in the presence of DTNB, a covalent allosteric inhibitor |
| 4M9I | A125C NS2B-NS3 protease from dengue virus 2 at pH 5.5 |
| 4M9K | NS2B-NS3 protease from dengue virus 2 at pH 5.5 |
| 4M9M | NS2B-NS3 protease from dengue virus 2 at pH 8.5 |
| 4M9F | Dengue virus 2 NS2B-NS3 protease A125C variant at pH 8.5 |
| 6MO1 | Structure of dengue virus 2 protease with an allosteric Inhibitor that blocks replication |
| 6MO2 | Structure of dengue virus 2 protease with an allosteric Inhibitor that blocks replication |
| 6MO0 | Structure of dengue virus 2 protease with an allosteric Inhibitor that blocks replication |

Figure S4. Published protein crystal structures of NS2B-NS3 proteases in DENV serotypes 1–4.

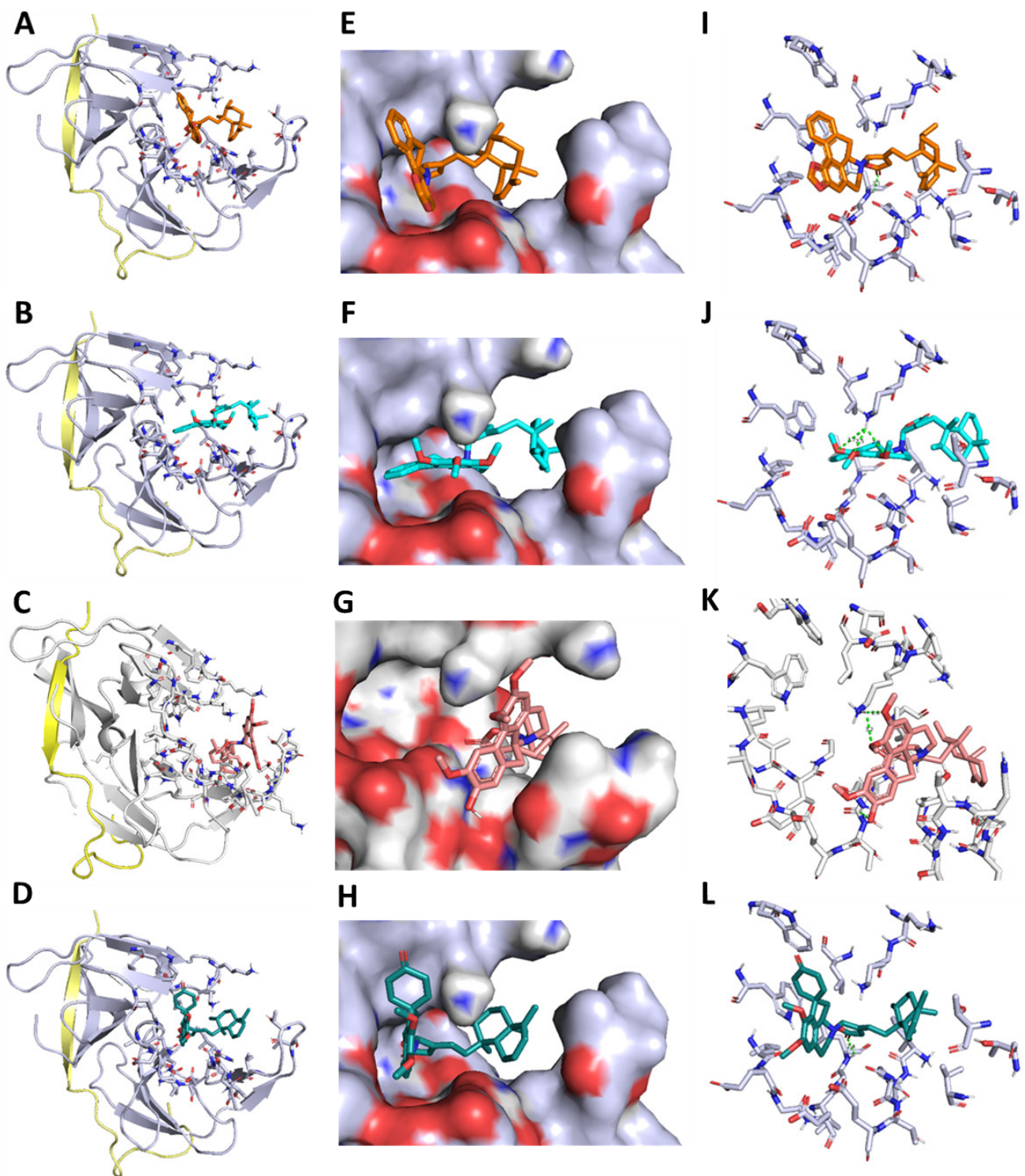


Figure S5. AutoDock 4.2 of binding simulation between DENV2 NS2B-NS3 protease (PDB ID: 6MO1) and compounds **1–4**. (A–D) Protein-polyallogarins **A–D** (**1–4**) complexes. Gray, NS3pro; yellow, NS2B; **1**, orange; **2**, cyan; **3**, peach; **4**, green. (E–H) Compounds **1–4** are individually located in the pocket of allosteric-site in the hydrophobicity surface model. (I–L) The hydrogen bond(s) between **1–4** and NS2B-NS3 protease in the allosteric pocket are shown in green dashed lines. All figures are made in

PyMOL 2.0.² Polyalongarins A-D (**1-4**) neither stay in the NS3pro active site (H51, D75, and S135) nor interact with NS2B (residues 48–71). Each of them enter into a pocket, in which Lys1074 regulates “opened-active” or “closed-inactive” forms of NS2B-NS3pro.³ In the DENV NS2B-NS3-polyalongarin A (**1**) complex, a H-bond between the α -NH group of Leu1149 and the O atom of C=O esteric carbonyl group (C-15) of **1** is observed within 2.1 Å. In the complex of DENV NS2B-NS3 protease and polyalongarin B (**2**), the ε -NH₂ group of Lys1074 associates with three O atoms of 1',2',3'-trimethoxyl groups of **2** through H-bonds within 3.7, 2.5, and 2.9 Å, respectively. In the DENV NS2B-NS3-polyalongarin C (**3**) complex, three H-bonds are found from the ε -NH₂ group of Lys1074 to the O atom of 1'-OMe (3.2 Å) and 2'-OMe (2.3 Å); and the γ -NH₂ group of Asn1167 to the O atoms of 11'-OH (2.2 Å). In the complex of DENV NS2B-NS3 protease and polyalongarin D (**4**), only one H-bond between the α -NH group of Leu1149 and the O atom of C=O esteric carbonyl group (C-15) of **4** is observed within 2.4 Å.

Table S1. Crystal data and structure refinement for **1**.

| | | |
|-----------------------------------|---|---|
| Identification code | d18480b | |
| Empirical formula | C37 H43 N O4 | |
| Formula weight | 565.72 | |
| Temperature | 200(2) K | |
| Wavelength | 1.54178 Å | |
| Crystal system | Monoclinic | |
| Space group | P 21 | |
| Unit cell dimensions | a = 12.2259(2) Å b = 9.50360(10) Å c = 13.0577(2) Å | α= 90°. β= 99.9780(10)°. γ = 90°. |
| Volume | 1494.23(4) Å ³ | |
| Z | 2 | |
| Density (calculated) | 1.257 Mg/m ³ | |
| Absorption coefficient | 0.635 mm ⁻¹ | |
| F(000) | 608 | |
| Crystal size | 0.20 x 0.11 x 0.05 mm ³ | |
| Theta range for data collection | 3.44 to 66.69°. | |
| Index ranges | -14<=h<=14, -11<=k<=11, -15<=l<=15 | |
| Reflections collected | 17601 | |
| Independent reflections | 5242 [R(int) = 0.0485] | |
| Completeness to theta = 66.69° | 99.5 % | |
| Absorption correction | multi-scan | |
| Max. and min. transmission | 0.9689 and 0.8835 | |
| Refinement method | Full-matrix least-squares on F ² | |
| Data / restraints / parameters | 5242 / 1 / 383 | |
| Goodness-of-fit on F ² | 1.044 | |
| Final R indices [I>2sigma(I)] | R1 = 0.0357, wR2 = 0.0905 | |
| R indices (all data) | R1 = 0.0383, wR2 = 0.0942 | |
| Absolute structure parameter | -0.02(17) | |
| Largest diff. peak and hole | 0.147 and -0.211 e.Å ⁻³ | |

Table S2. Atomic coordinates and equivalent isotropic displacement parameters for **1**. U(eq) is defined as one third of the trace of the orthogonalized U tensor.

| | x | y | z | U(eq) |
|-------|----------|---------|---------|-------|
| C(1) | 4920(1) | 8975(2) | 1248(1) | 34(1) |
| C(2) | 6001(1) | 8318(2) | 1203(1) | 32(1) |
| C(3) | 6170(1) | 7253(2) | 1858(1) | 29(1) |
| C(4) | 7113(1) | 6237(2) | 2089(1) | 34(1) |
| C(5) | 8185(1) | 6777(2) | 1771(2) | 33(1) |
| C(6) | 9224(1) | 5804(2) | 2008(1) | 29(1) |
| C(7) | 10124(2) | 6517(2) | 1494(2) | 43(1) |
| C(8) | 9603(1) | 5686(2) | 3207(2) | 38(1) |
| C(9) | 10032(2) | 7052(3) | 3748(2) | 60(1) |
| C(10) | 10484(2) | 4535(2) | 3495(2) | 45(1) |
| C(11) | 10142(2) | 3111(2) | 3028(2) | 42(1) |
| C(12) | 9822(1) | 3157(2) | 1833(1) | 31(1) |
| C(13) | 10877(1) | 3372(2) | 1339(2) | 41(1) |
| C(14) | 9319(2) | 1747(2) | 1433(2) | 39(1) |
| C(15) | 9891(2) | 437(2) | 1875(2) | 58(1) |
| C(16) | 8422(2) | 1656(2) | 703(2) | 47(1) |
| C(17) | 7801(2) | 2870(2) | 170(2) | 50(1) |
| C(18) | 8415(2) | 4250(2) | 411(1) | 38(1) |
| C(19) | 8915(1) | 4310(2) | 1570(1) | 27(1) |
| C(20) | 5231(1) | 7192(2) | 2473(1) | 30(1) |
| C(21) | 4252(2) | 5222(2) | 1531(1) | 34(1) |
| C(22) | 4247(2) | 3640(2) | 1649(1) | 39(1) |
| C(23) | 3799(1) | 3189(2) | 2604(1) | 31(1) |
| C(24) | 3689(1) | 4145(2) | 3390(1) | 28(1) |
| C(25) | 3987(1) | 5690(2) | 3296(1) | 28(1) |
| C(26) | 4505(1) | 6269(2) | 4356(1) | 37(1) |
| C(27) | 3777(1) | 6000(2) | 5157(1) | 32(1) |
| C(28) | 3729(2) | 6977(2) | 5938(1) | 38(1) |
| C(29) | 3100(2) | 6714(2) | 6710(1) | 42(1) |
| C(30) | 2526(2) | 5465(2) | 6697(1) | 41(1) |
| C(31) | 2564(2) | 4482(2) | 5922(1) | 37(1) |
| C(32) | 3194(1) | 4736(2) | 5137(1) | 30(1) |
| C(33) | 3272(1) | 3719(2) | 4297(1) | 29(1) |
| C(34) | 2968(1) | 2324(2) | 4323(1) | 32(1) |
| C(35) | 2249(2) | 248(2) | 4682(2) | 47(1) |
| C(36) | 3095(2) | 1373(2) | 3549(1) | 35(1) |
| C(37) | 3512(2) | 1762(2) | 2682(1) | 37(1) |
| N(1) | 4744(1) | 5848(2) | 2533(1) | 30(1) |
| O(1) | 4466(1) | 9952(2) | 761(1) | 48(1) |
| O(2) | 4451(1) | 8278(1) | 1980(1) | 36(1) |
| O(3) | 2566(1) | 1602(1) | 5112(1) | 42(1) |
| O(4) | 2784(1) | 36(2) | 3812(1) | 51(1) |

Table S3. The Predicted Binding Affinity and RMSD bounds of **1–4**.

| Ligand & Energy Minimization | Binding Affinity (kcal/mol) | Mode | RMSD lower bound | RMSD upper bound |
|------------------------------|-----------------------------|------|------------------|------------------|
| cpd_1_uff_E=949.78 | -10.2 | 0 | 0 | 0 |
| cpd_1_uff_E=949.78 | -10.2 | 1 | 0.954 | 2.48 |
| cpd_1_uff_E=949.78 | -10 | 2 | 1.116 | 2.038 |
| cpd_1_uff_E=949.78 | -10 | 3 | 3.771 | 9.962 |
| cpd_1_uff_E=949.78 | -9.8 | 4 | 2.28 | 8.337 |
| cpd_1_uff_E=949.78 | -9.7 | 5 | 2.789 | 4.971 |
| cpd_1_uff_E=949.78 | -9.6 | 6 | 6.388 | 11.439 |
| cpd_1_uff_E=949.78 | -9.5 | 7 | 2.516 | 4.412 |
| cpd_1_uff_E=949.78 | -9.4 | 8 | 4.716 | 8.426 |
| cpd_2_uff_E=1094.59 | -9.2 | 0 | 0 | 0 |
| cpd_2_uff_E=1094.59 | -8.7 | 1 | 1.209 | 2.171 |
| cpd_2_uff_E=1094.59 | -8.3 | 2 | 1.708 | 3.228 |
| cpd_2_uff_E=1094.59 | -7.9 | 3 | 2.441 | 5.109 |
| cpd_2_uff_E=1094.59 | -7.9 | 4 | 1.48 | 3.303 |
| cpd_2_uff_E=1094.59 | -7.8 | 5 | 1.2 | 1.974 |
| cpd_2_uff_E=1094.59 | -7.6 | 6 | 2.591 | 5.318 |
| cpd_2_uff_E=1094.59 | -7.2 | 7 | 3.701 | 9.774 |
| cpd_2_uff_E=1094.59 | -7.2 | 8 | 4.396 | 9.393 |
| cpd_3_uff_E=961.60 | -8.9 | 0 | 0 | 0 |
| cpd_3_uff_E=961.60 | -8.7 | 1 | 6.587 | 11.565 |
| cpd_3_uff_E=961.60 | -8.1 | 2 | 6.22 | 10.061 |
| cpd_3_uff_E=961.60 | -8.1 | 3 | 5.914 | 10.884 |
| cpd_3_uff_E=961.60 | -8.0 | 4 | 8.32 | 12.125 |
| cpd_3_uff_E=961.60 | -8.0 | 5 | 7.674 | 11.566 |
| cpd_3_uff_E=961.60 | -7.9 | 6 | 6.616 | 10.599 |
| cpd_3_uff_E=961.60 | -7.9 | 7 | 0.964 | 2.433 |
| cpd_3_uff_E=961.60 | -7.7 | 8 | 3.134 | 9.493 |
| cpd_4_uff_E=945.54 | -9.8 | 0 | 0 | 0 |
| cpd_4_uff_E=945.54 | -9.4 | 1 | 2.831 | 9.192 |
| cpd_4_uff_E=945.54 | -9.3 | 2 | 5.743 | 10.916 |
| cpd_4_uff_E=945.54 | -9.0 | 3 | 8.264 | 11.236 |
| cpd_4_uff_E=945.54 | -8.9 | 4 | 4.42 | 7.09 |
| cpd_4_uff_E=945.54 | -8.9 | 5 | 3.112 | 9.452 |
| cpd_4_uff_E=945.54 | -8.6 | 6 | 6.809 | 12.177 |
| cpd_4_uff_E=945.54 | -8.6 | 7 | 5.625 | 11.213 |
| cpd_4_uff_E=945.54 | -8.6 | 8 | 2.549 | 9.904 |

Table S4. Python Shell Information of 1–4 in Different Models.

Python 2.6.5 (r265:79096, Mar 19 2010, 21:48:26) [MSC v.1500 32 bit (Intel)] on win32

Type "help", "copyright", "credits" or "license" for more information.

adding gasteiger charges to peptide

cpd_1_uff_E=949.78_out_model1 : -10.2 , 0.0 , 0.0
cpd_1_uff_E=949.78_out_model2 : -10.2 , 0.954 , 2.48
cpd_1_uff_E=949.78_out_model3 : -10.0 , 1.116 , 2.038
cpd_1_uff_E=949.78_out_model4 : -10.0 , 3.771 , 9.962
cpd_1_uff_E=949.78_out_model5 : -9.8 , 2.28 , 8.337
cpd_1_uff_E=949.78_out_model6 : -9.7 , 2.789 , 4.971
cpd_1_uff_E=949.78_out_model7 : -9.6 , 6.388 , 11.439
cpd_1_uff_E=949.78_out_model8 : -9.5 , 2.516 , 4.412
cpd_1_uff_E=949.78_out_model9 : -9.4 , 4.716 , 8.426
cpd_2_uff_E=1094.59_out_model1 : -9.2 , 0.0 , 0.0
cpd_2_uff_E=1094.59_out_model2 : -8.7 , 1.209 , 2.171
cpd_2_uff_E=1094.59_out_model3 : -8.3 , 1.708 , 3.228
cpd_2_uff_E=1094.59_out_model4 : -7.9 , 2.441 , 5.109
cpd_2_uff_E=1094.59_out_model5 : -7.9 , 1.48 , 3.303
cpd_2_uff_E=1094.59_out_model6 : -7.8 , 1.2 , 1.974
cpd_2_uff_E=1094.59_out_model7 : -7.6 , 2.591 , 5.318
cpd_2_uff_E=1094.59_out_model8 : -7.2 , 3.701 , 9.774
cpd_2_uff_E=1094.59_out_model9 : -7.2 , 4.396 , 9.393
cpd_3_uff_E=961.60_out_model1 : -8.9 , 0.0 , 0.0
cpd_3_uff_E=961.60_out_model2 : -8.7 , 6.615 , 11.486
cpd_3_uff_E=961.60_out_model3 : -8.0 , 8.306 , 12.001
cpd_3_uff_E=961.60_out_model4 : -8.0 , 0.954 , 2.474
cpd_3_uff_E=961.60_out_model5 : -8.0 , 5.978 , 9.748
cpd_3_uff_E=961.60_out_model6 : -7.9 , 9.125 , 13.527
cpd_3_uff_E=961.60_out_model7 : -7.8 , 11.507 , 16.863
cpd_3_uff_E=961.60_out_model8 : -7.8 , 8.653 , 10.883
cpd_3_uff_E=961.60_out_model9 : -7.8 , 2.032 , 4.046
cpd_4_uff_E=945.54_out_model1 : -9.8 , 0.0 , 0.0
cpd_4_uff_E=945.54_out_model2 : -9.4 , 2.831 , 9.192
cpd_4_uff_E=945.54_out_model3 : -9.3 , 5.743 , 10.916
cpd_4_uff_E=945.54_out_model4 : -9.0 , 8.264 , 11.236
cpd_4_uff_E=945.54_out_model5 : -8.9 , 4.42 , 7.09
cpd_4_uff_E=945.54_out_model6 : -8.9 , 3.112 , 9.452
cpd_4_uff_E=945.54_out_model7 : -8.6 , 6.809 , 12.177
cpd_4_uff_E=945.54_out_model8 : -8.6 , 5.625 , 11.213
cpd_4_uff_E=945.54_out_model9 : -8.6 , 2.549 , 9.904

References

- (1) (a) Misra, P.; Sashidhara, K. V.; Singh, S. P.; Kumar, A.; Gupta, R.; Chaudhaery, S. S.; Gupta, S. S.; Majumder, H. K.; Saxena, A. K.; Dube, A. 16 α -Hydroxycleroda-3,13(14)Z-dien-15,16-olide from *Polyalthia longifolia*: a safe and orally active antileishmanial agent inflammation. *Br. J. Pharmacol.* **2010**, *159*, 1143–1150. (b) Potter, K. C.; Zi, J. C.; Hong, Y. J.; Schulte, S.; Malchow, B.; Tantillo, D. J.; Peters, R. J. Blocking Deprotonation with Retention of Aromaticity in a Plant *ent*-Copalyl Diphosphate Synthase Leads to Product Rearrangement. *Angew. Chem. Int. Ed.* **2016**, *55*, 634–638. (c) Yang, M.; Zhu, L. P.; Li, L.; Li, J. J.; Xu, L. M.; Feng, J.; Liu, Y. L. Digital Gene Expression Analysis Provides Insight into the Transcript Profile of the Genes Involved in Aporphine Alkaloid Biosynthesis in Lotus (*Nelumbo nucifera*). *Front. Plant Sci.* **2017**, *8*, 80. (d) Hirata K.; Poeaknapo C.; Schmidt J. Zenk M.H. 1,2-Dehydroreticuline synthase, the branch point enzyme opening the morphinan biosynthetic pathway. *Phytochemistry* **2004**, *65*, 1039–1046. (e) De-Eknamkul W. and Zenk M.H. Purification and properties of 1,2-dehydroreticuline reductase from *Papaver somniferum* seedlings. *Phytochemistry* **1992**, *31*, 813–821.
- (2) The PyMOL Molecular Graphics System, Version 2.0 Schrödinger, LLC. (<https://pymol.org/2/>)
- (3) (a) Erbel, P.; Schiering, N.; D’Arcy, A.; Renatus, M.; Kroemer, M.; Lim, S. P.; Yin, Z.; Keller, T. H.; Vasudevan, S. G.; Hommel, U. Structural basis for the activation of flaviviral NS3 proteases from dengue and West Nile virus. *Nat. Struct. Mol. Biol.* **2006**, *13*, 372–373. (b) Yildiz, M.; Ghosh, S.; Bell, J. A.; Sherman, W.; Hardy, J. A. Allosteric Inhibition of the NS2B-NS3 Protease from Dengue Virus. *ACS Chem. Biol.* **2013**, *8*, 2744–2752. (c) Yao, Y.; Huo, T.; Lin, Y. L.; Nie, S. Y.; Wu, F. R.; Hua, Y. D.; Wu, J. Y.; Kneubehl, A. R.; Vogt, M. B.; Rico-Hesse, R.; Song, Y. C. Discovery, X-ray Crystallography and Antiviral Activity of Allosteric Inhibitors of Flavivirus NS2B-NS3 Protease. *J. Am. Chem. Soc.* **2019**, *141*, 6832–6836.

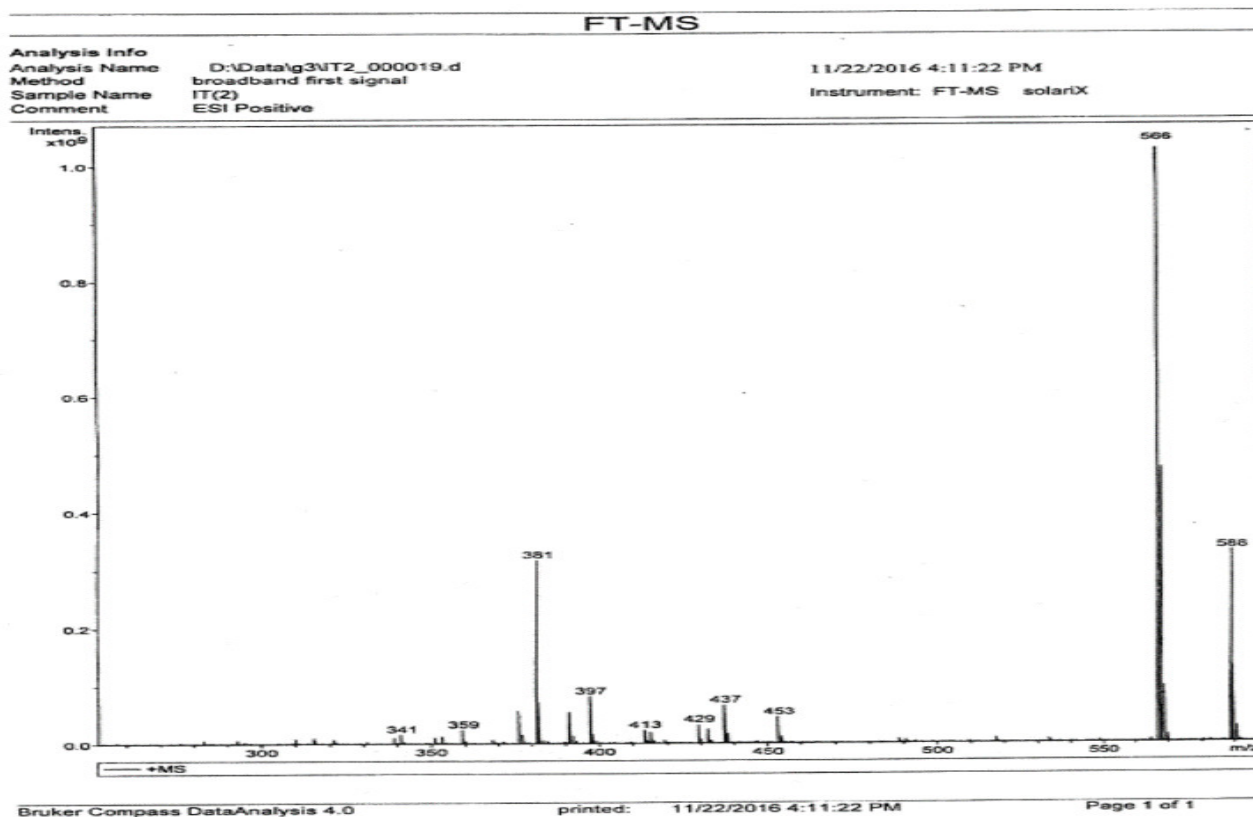


Figure PA-1. ESI-MS spectrum of polyalongarin A (1)

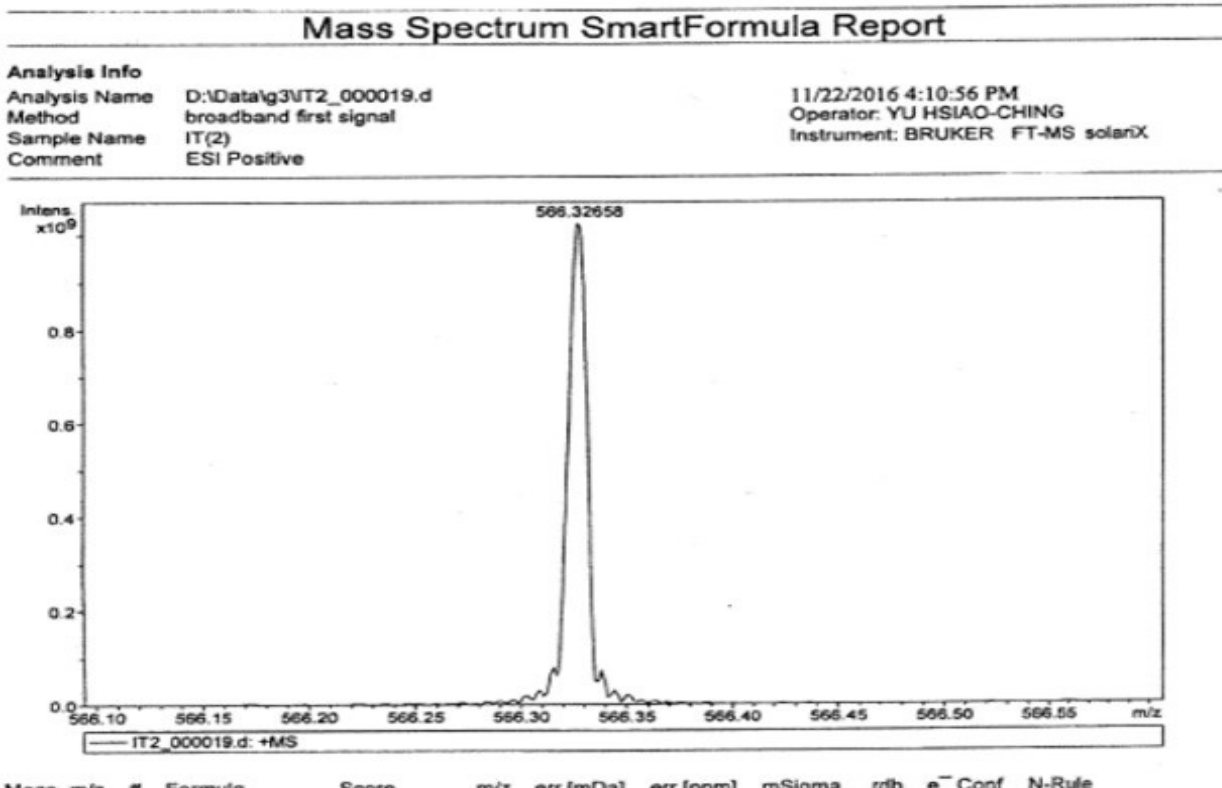


Figure PA-2. HR-ESI-MS spectrum of polyalongarin A (1)

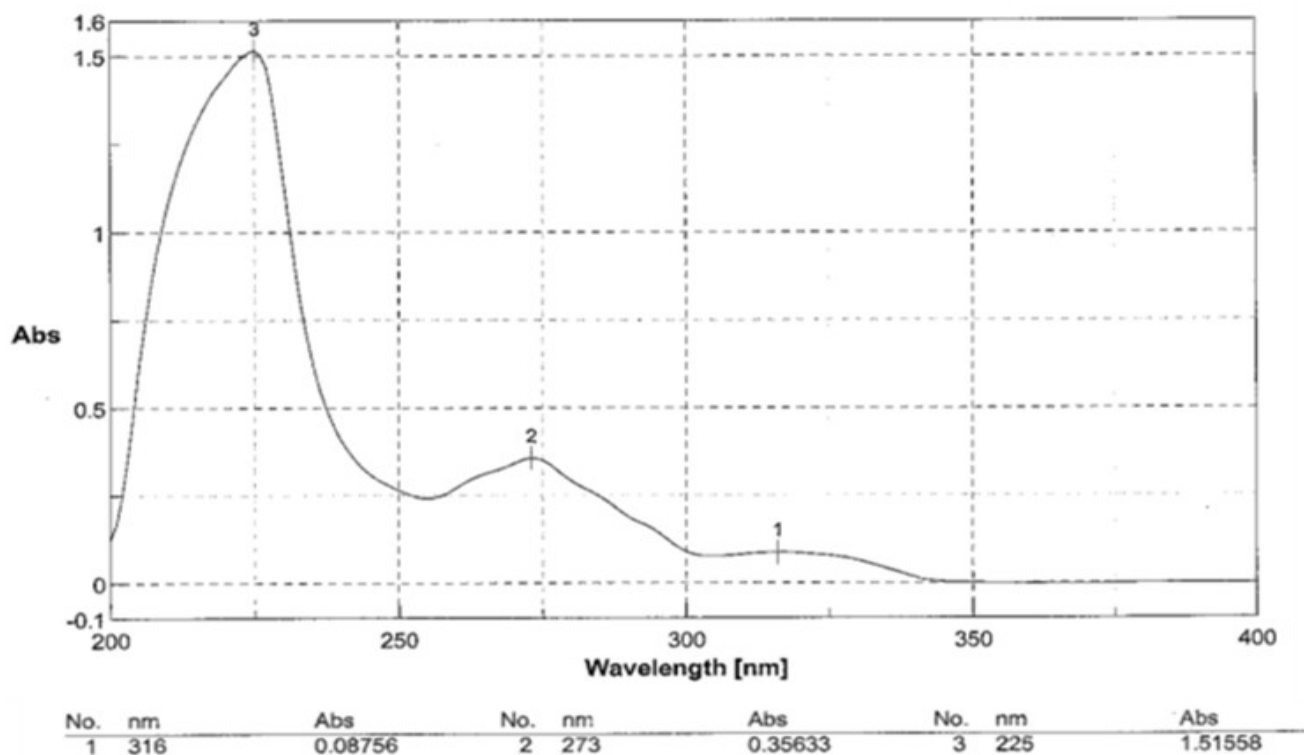
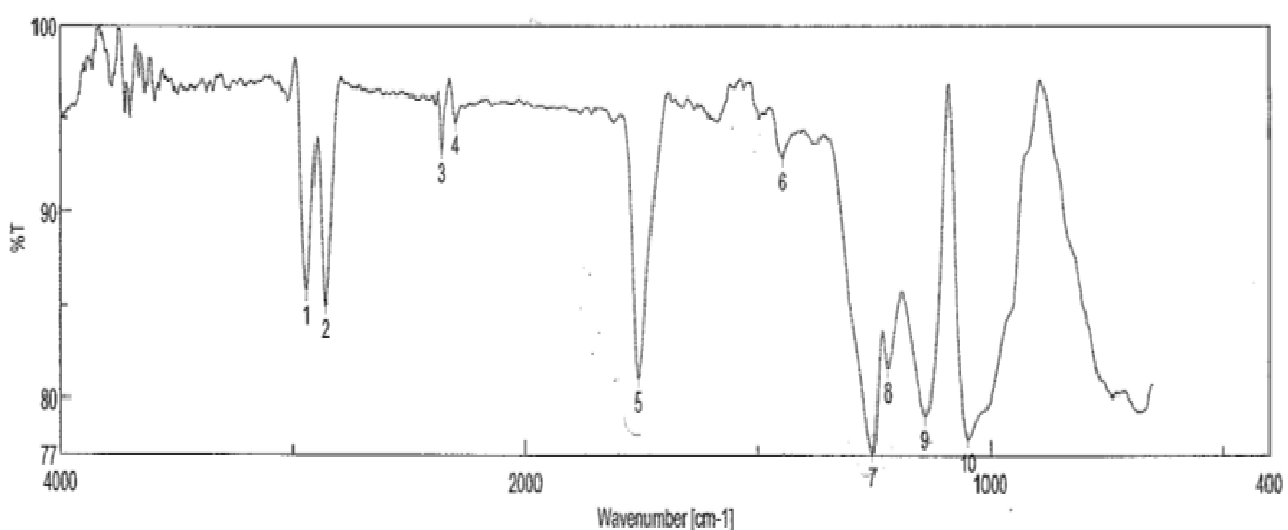


Figure PA-3. UV spectrum of polyalongirin A (1)



[Result of Peak Picking]

| No. | Position | Intensity | No. | Position | Intensity | No. | Position | Intensity |
|-----|----------|-----------|-----|----------|-----------|-----|----------|-----------|
| 1 | 2939.95 | 85.7378 | 2 | 2860.88 | 84.9666 | 3 | 2361.41 | 93.251 |
| 4 | 2300.66 | 94.8141 | 5 | 1755.87 | 81.0985 | 6 | 1447.31 | 92.8378 |
| 7 | 1252.54 | 77.0856 | 8 | 1220.72 | 81.6289 | 9 | 1139.72 | 79.1067 |
| 10 | 1047.16 | 77.8573 | | | | | | |

Figure PA-4. IR spectrum of polyalongirin A (1)

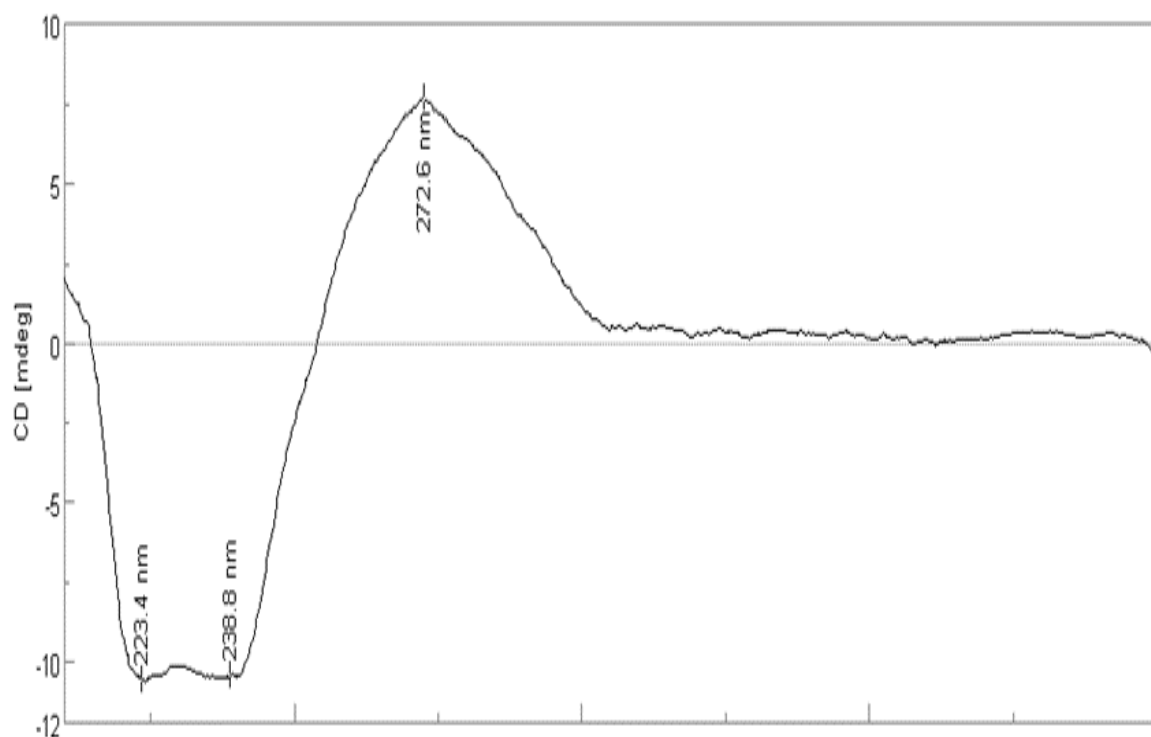


Figure PA-5. CD spectrum of polyalongarin A (**1**)

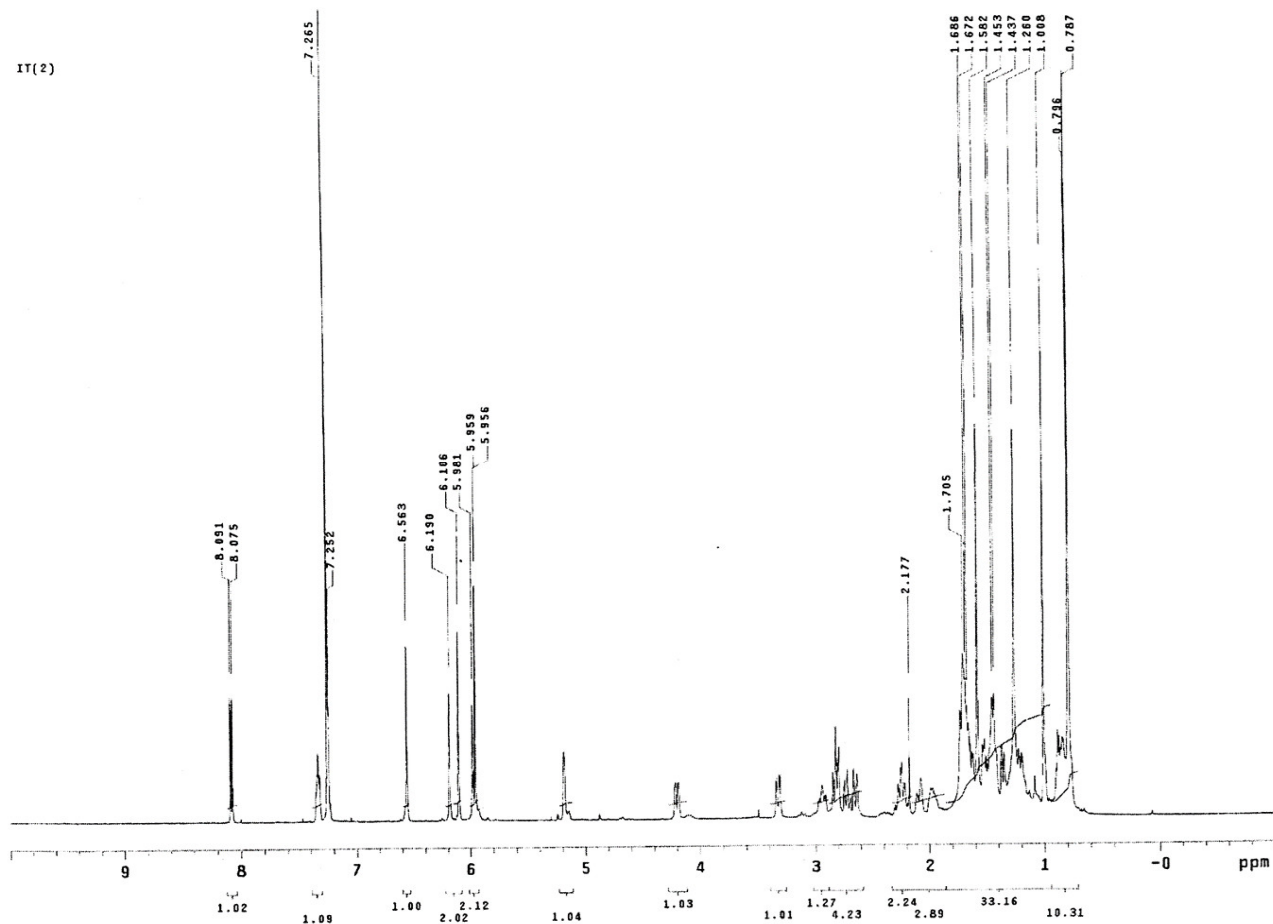


Figure PA-6. ^1H -NMR spectrum of polyalongarin A (**1**) in CDCl_3 (500 MHz)

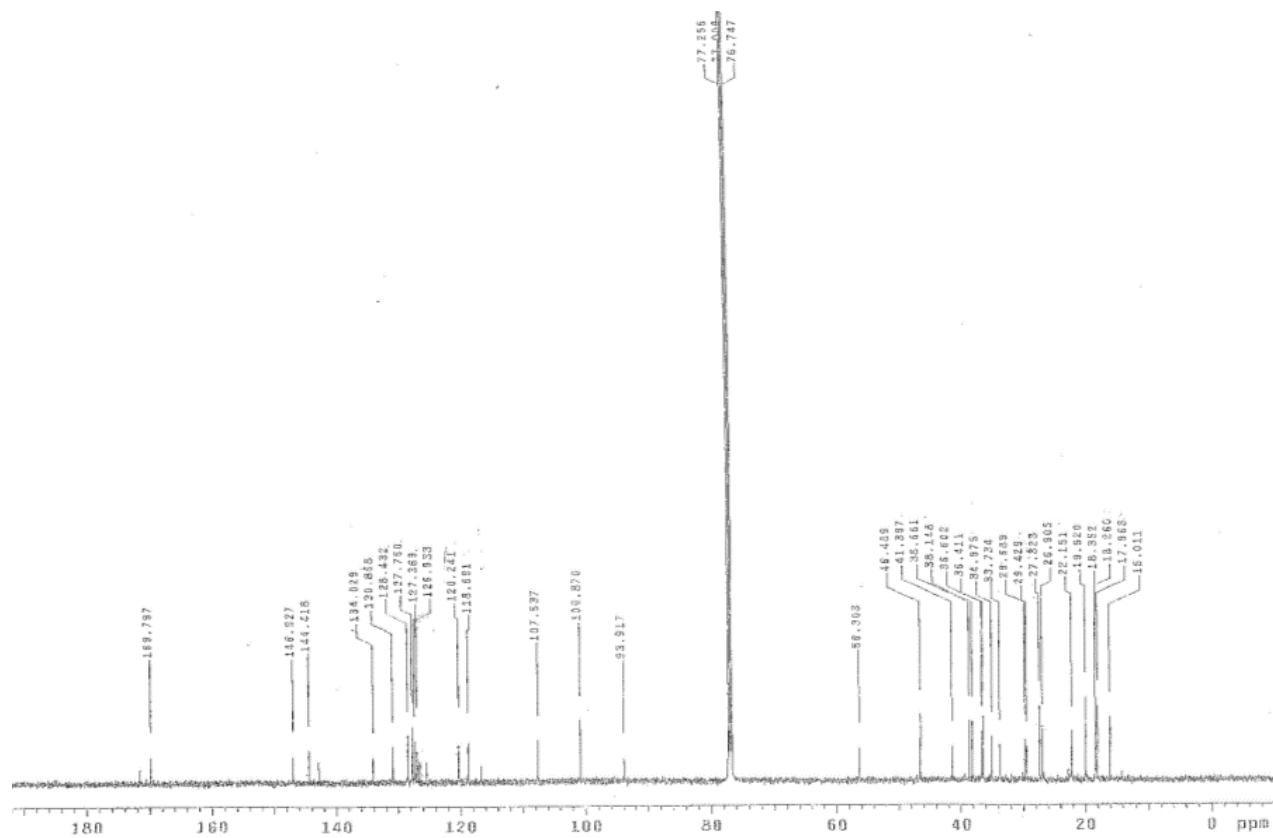


Figure PA-7. ^{13}C -NMR spectrum of polyalongarin A (**1**) in CDCl_3 (125 MHz)

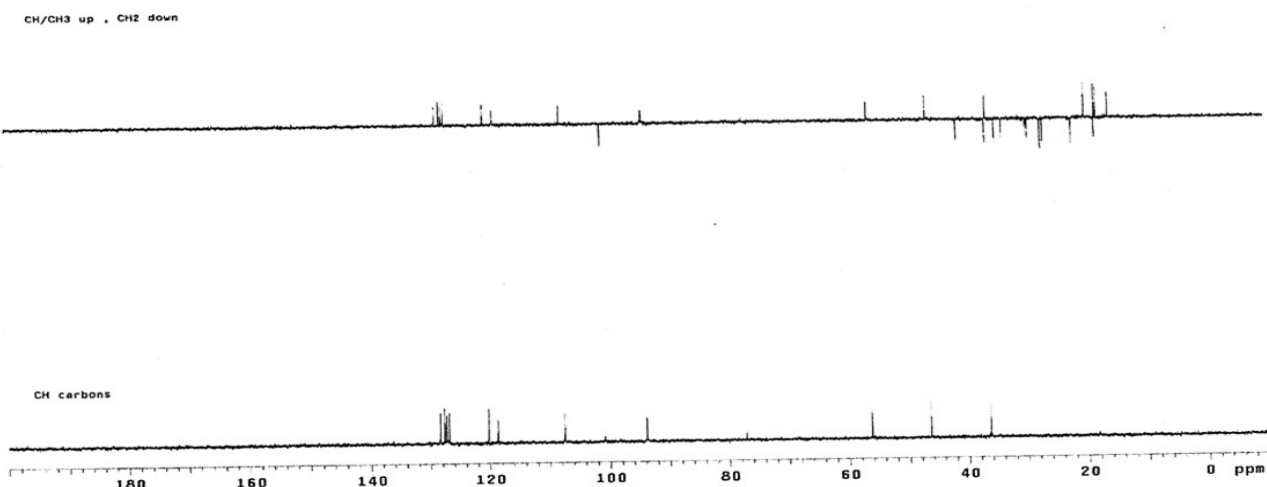


Figure PA-8. DEPT-135 and DEPT-90 spectra of polyalongarin A (**1**)

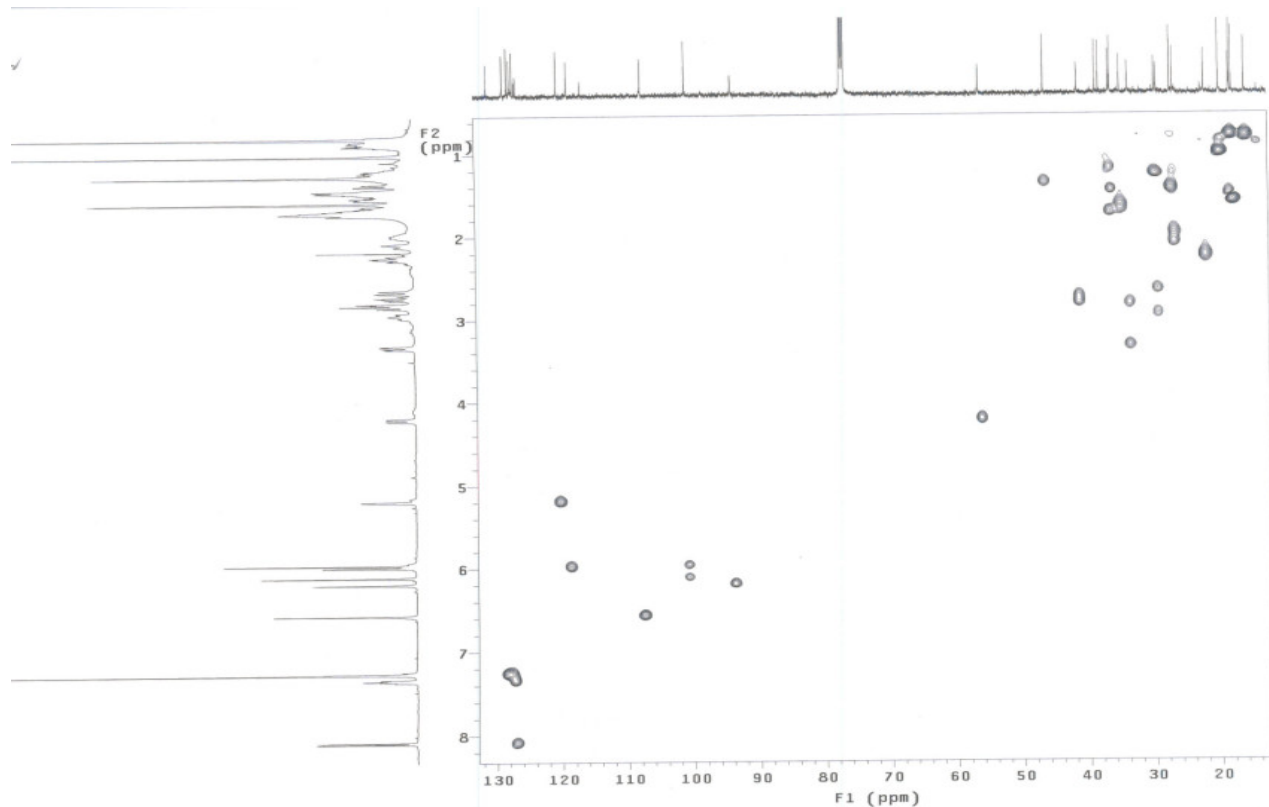


Figure PA-9. HMQC spectrum of polyalongarin A (1)

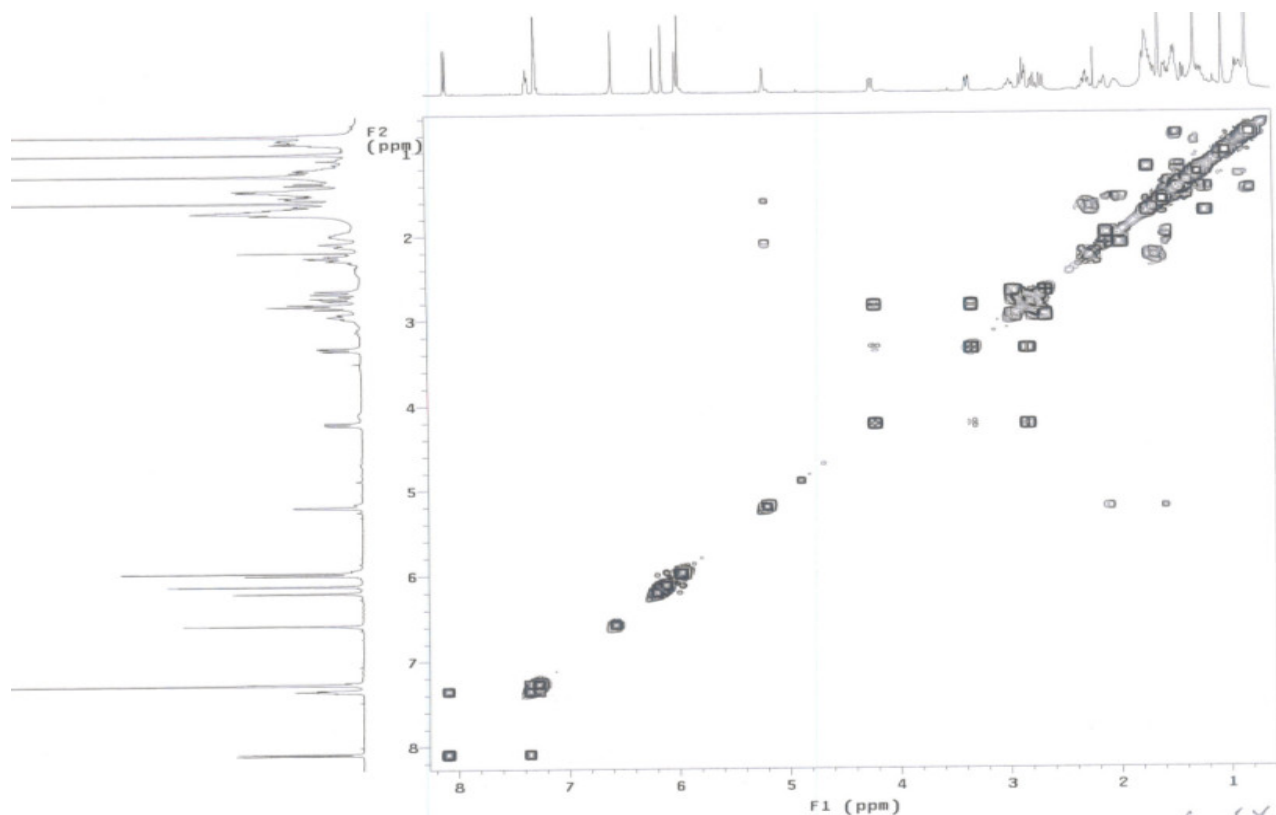


Figure PA-10. COSY spectrum of polyalongarin A (1)

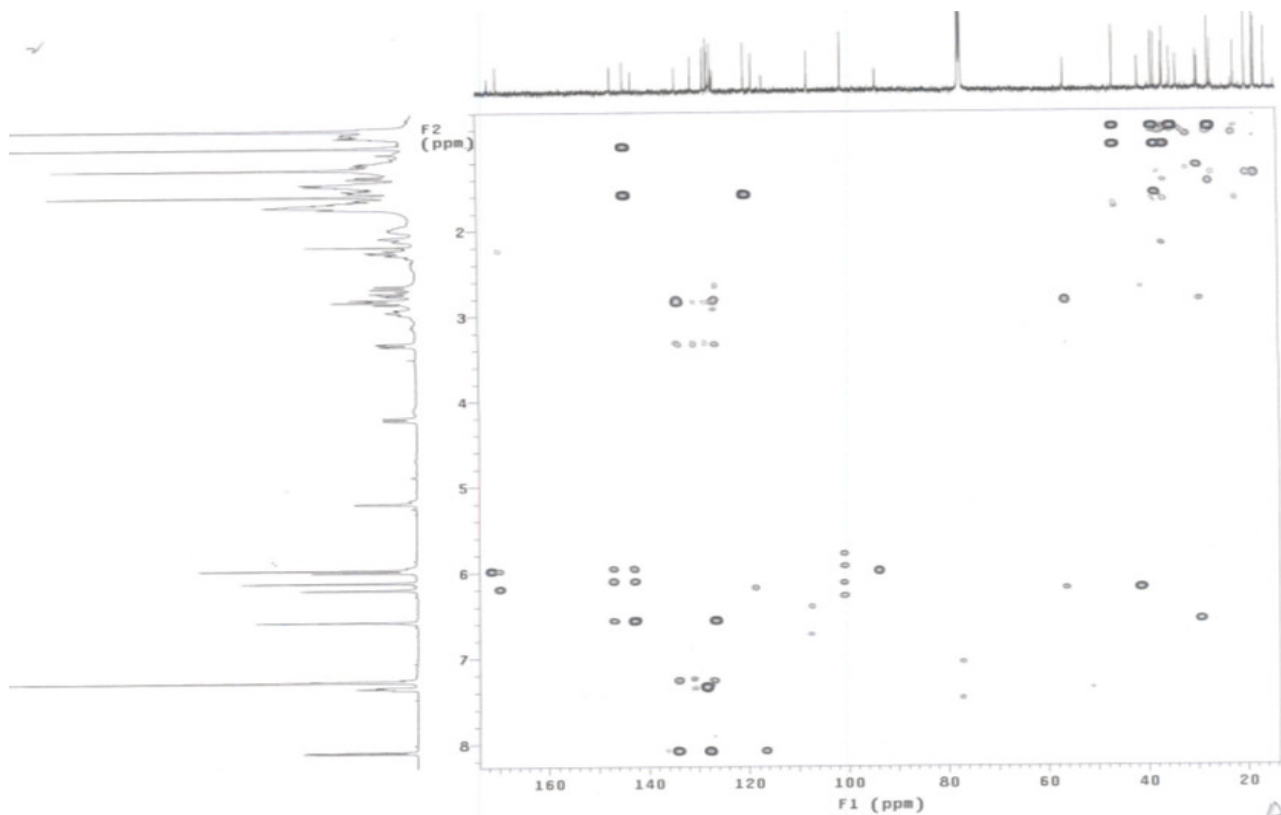


Figure PA-11. HMBC spectrum of polyalongarin A (1)

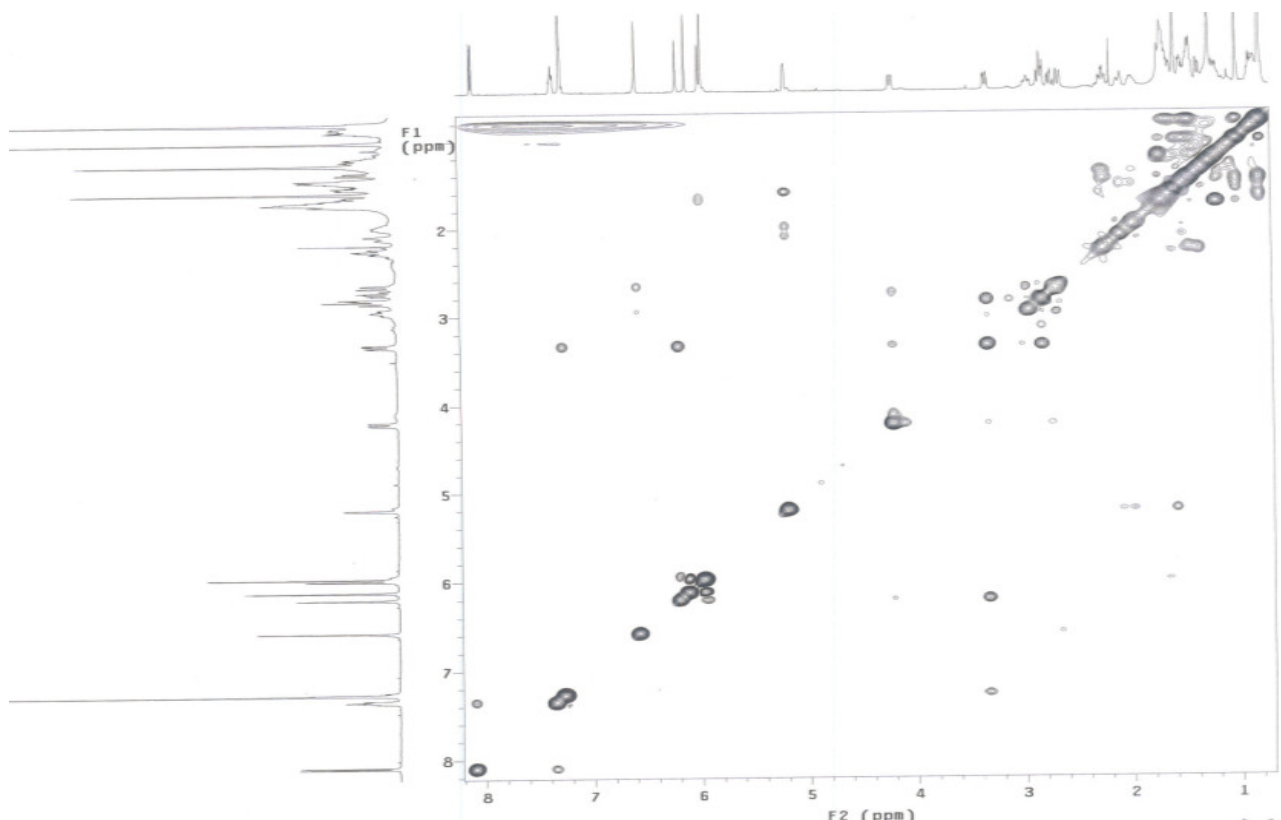
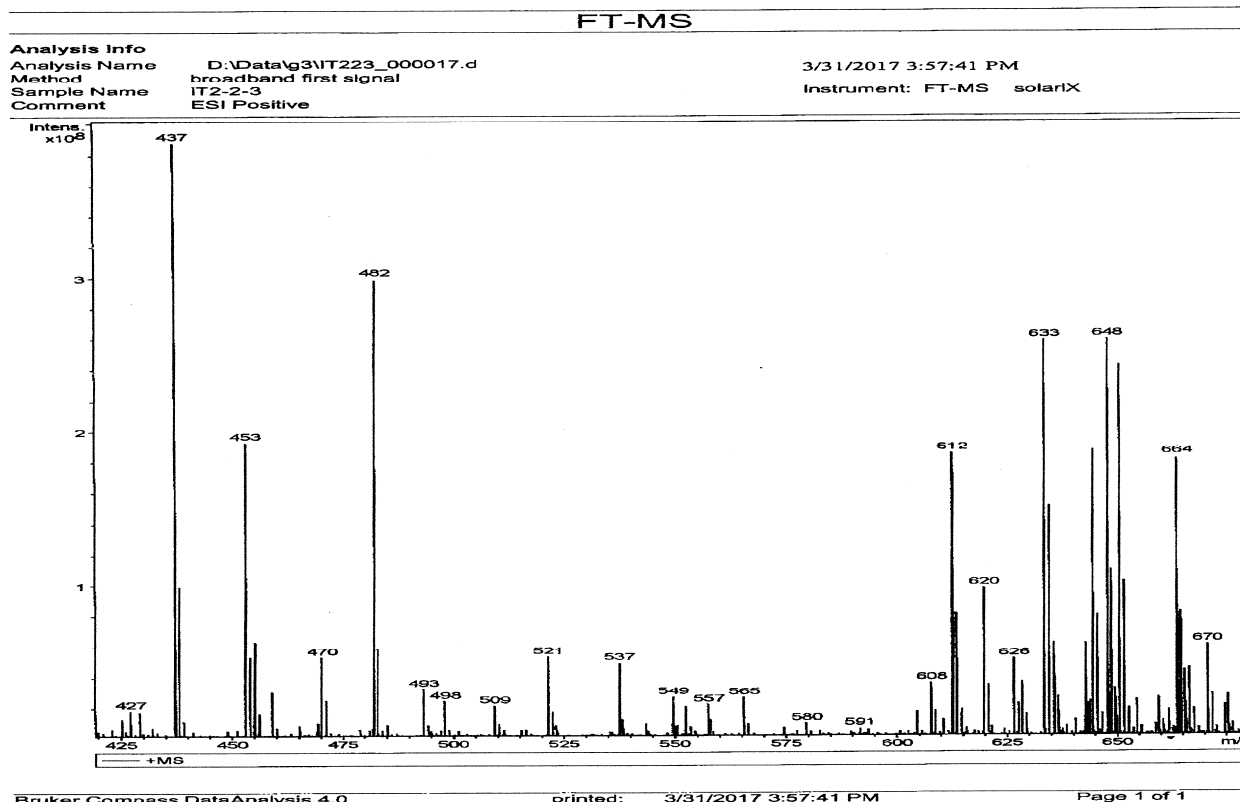
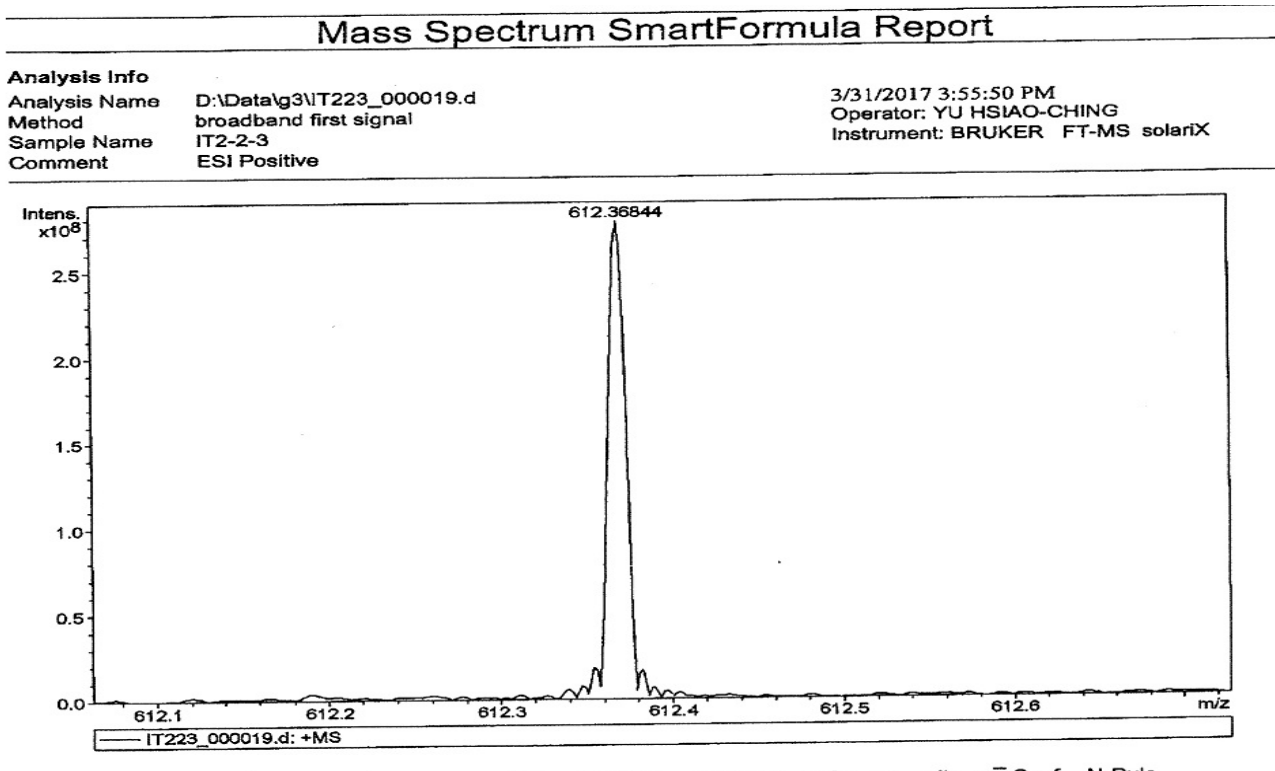


Figure PA-12. NOESY spectrum of polyalongarin A (1)



Bruker Compass DataAnalysis 4.0 printed: 3/31/2017 3:57:41 PM Page 1 of 1

Figure PB-1. ESI-MS spectrum of polyalongarin B (2)



| Meas. m/z | # | Formula | Score | m/z | err [mDa] | err [ppm] | mSigma | rdb | e ⁻ Conf | N-Rule |
|-----------|---|-----------------|--------|-----------|-----------|-----------|--------|------|---------------------|--------|
| 612.36844 | 1 | C 39 H 50 N O 5 | 100.00 | 612.36835 | -0.09 | -0.15 | 15.2 | 15.5 | even | ok |

Figure PB-2. HR-ESI-MS spectrum of polyalongarin B (2)

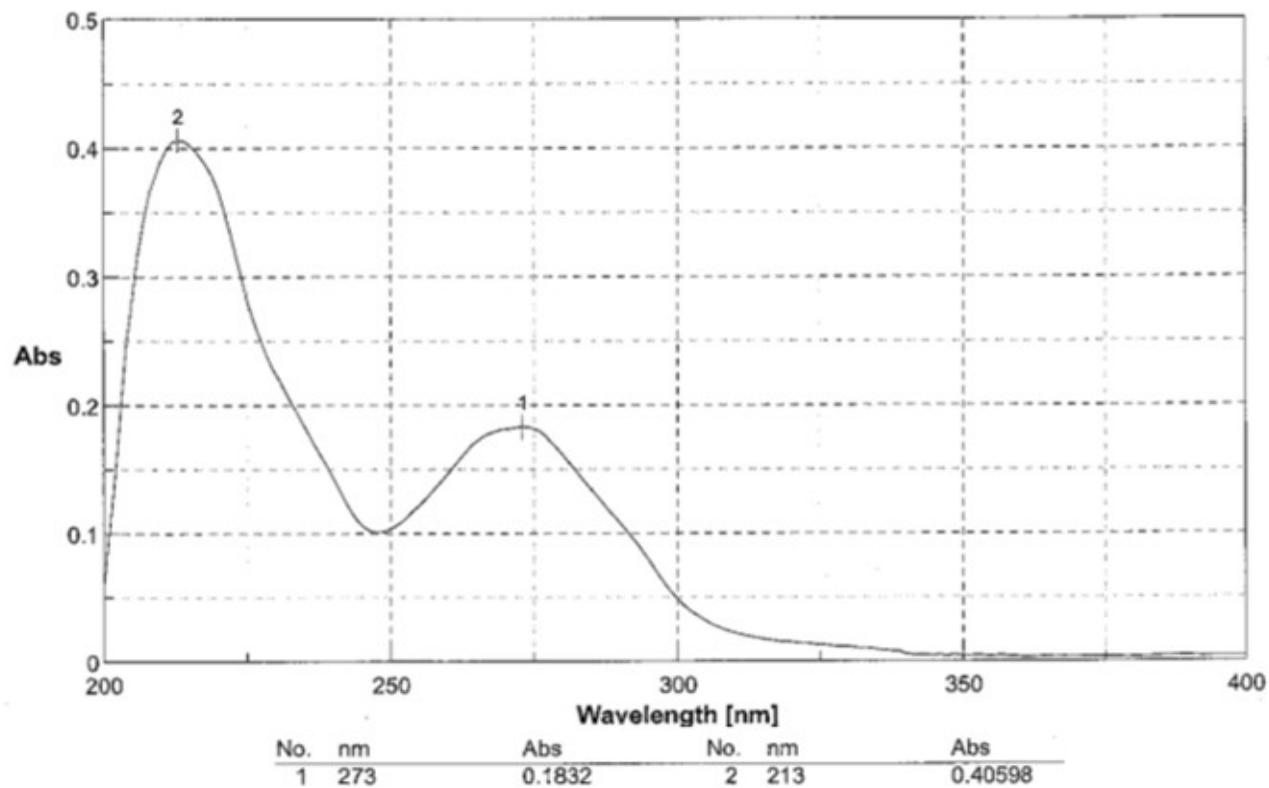


Figure PB-3. UV spectrum of polyalongarin B (2)

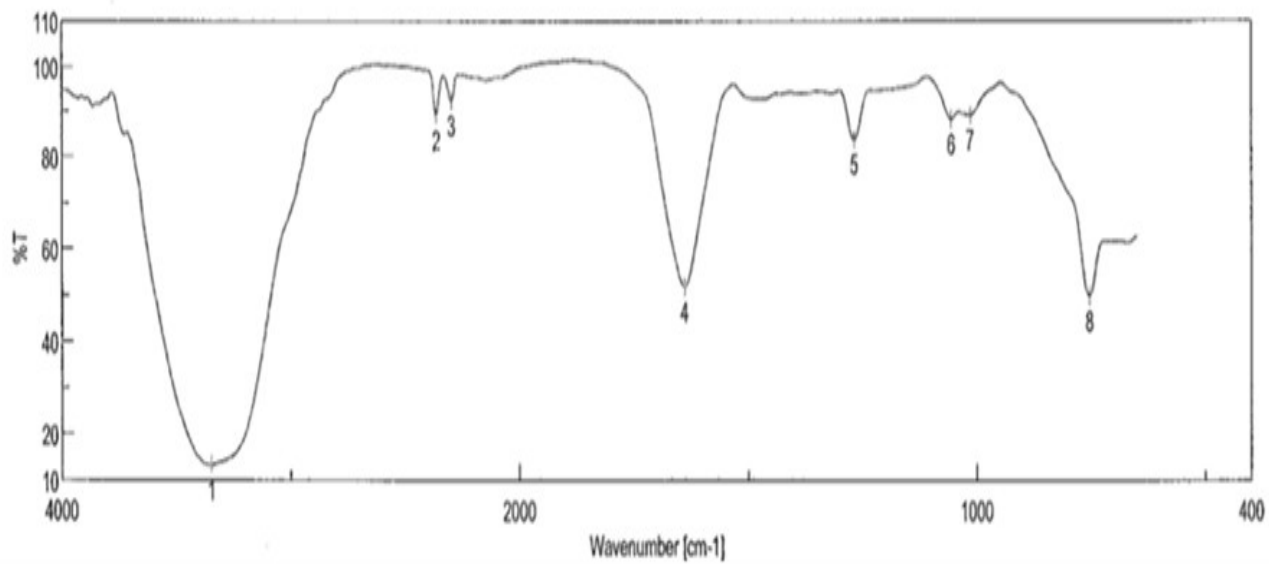


Figure PB-4. IR spectrum of polyalongarin B (2)

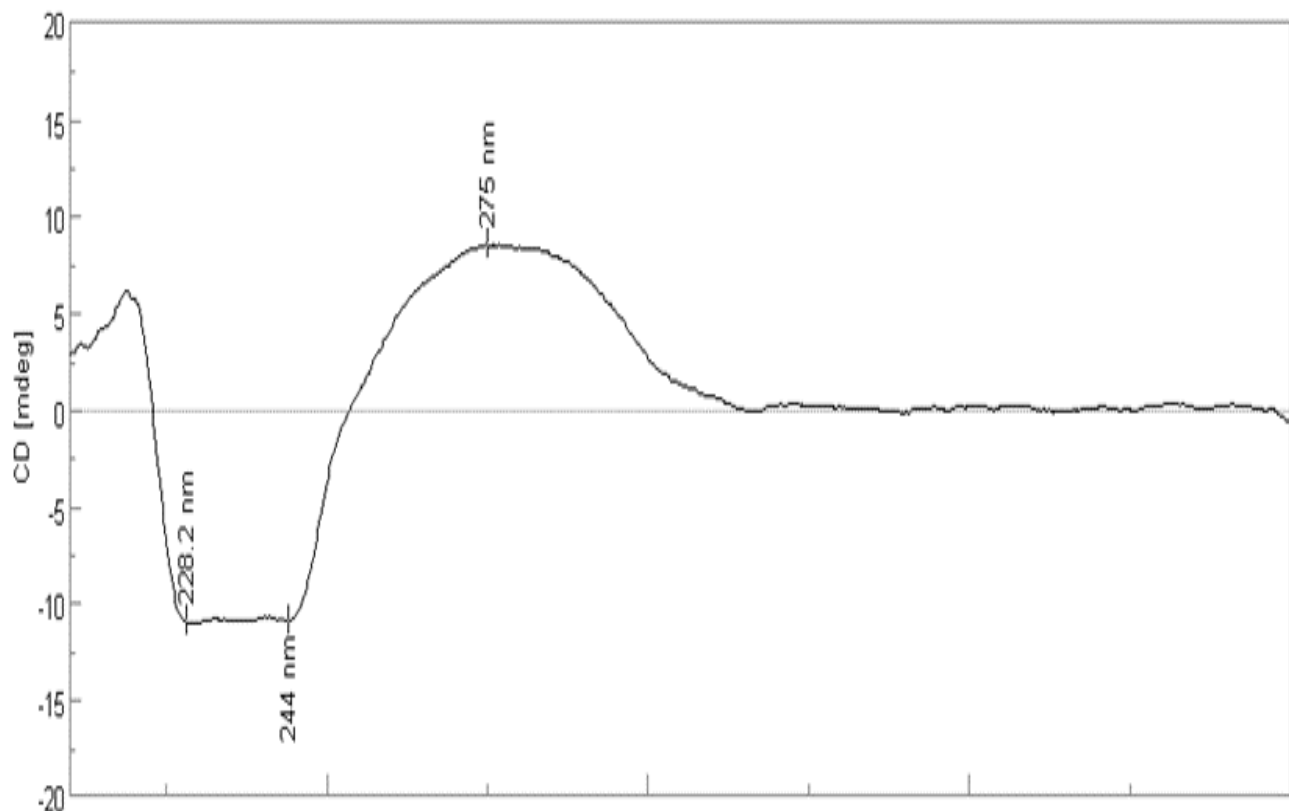


Figure PB-5. CD spectrum of polyalongarin B (2)

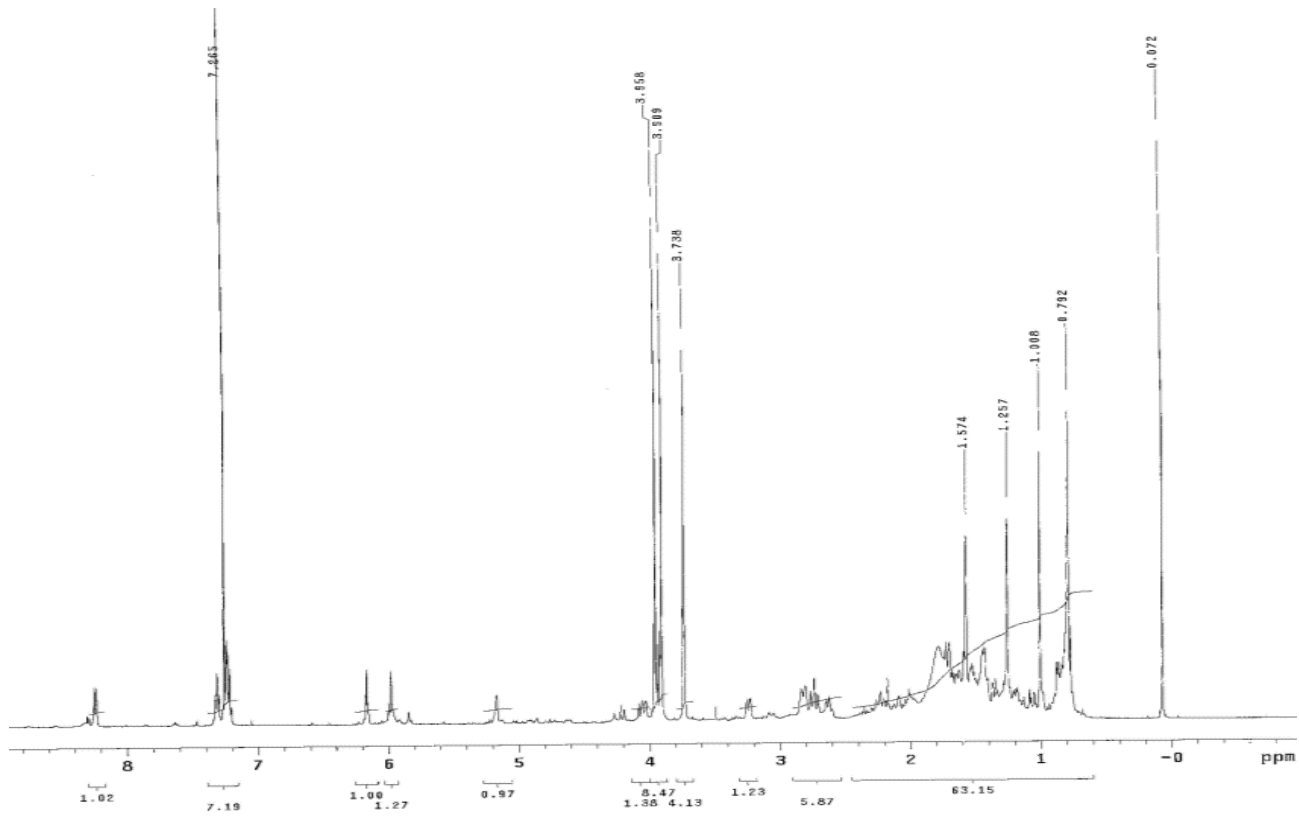


Figure PB-6. ¹H-NMR spectrum of polyalongarin B (2) in CDCl₃ (500 MHz)

1T2-2-3

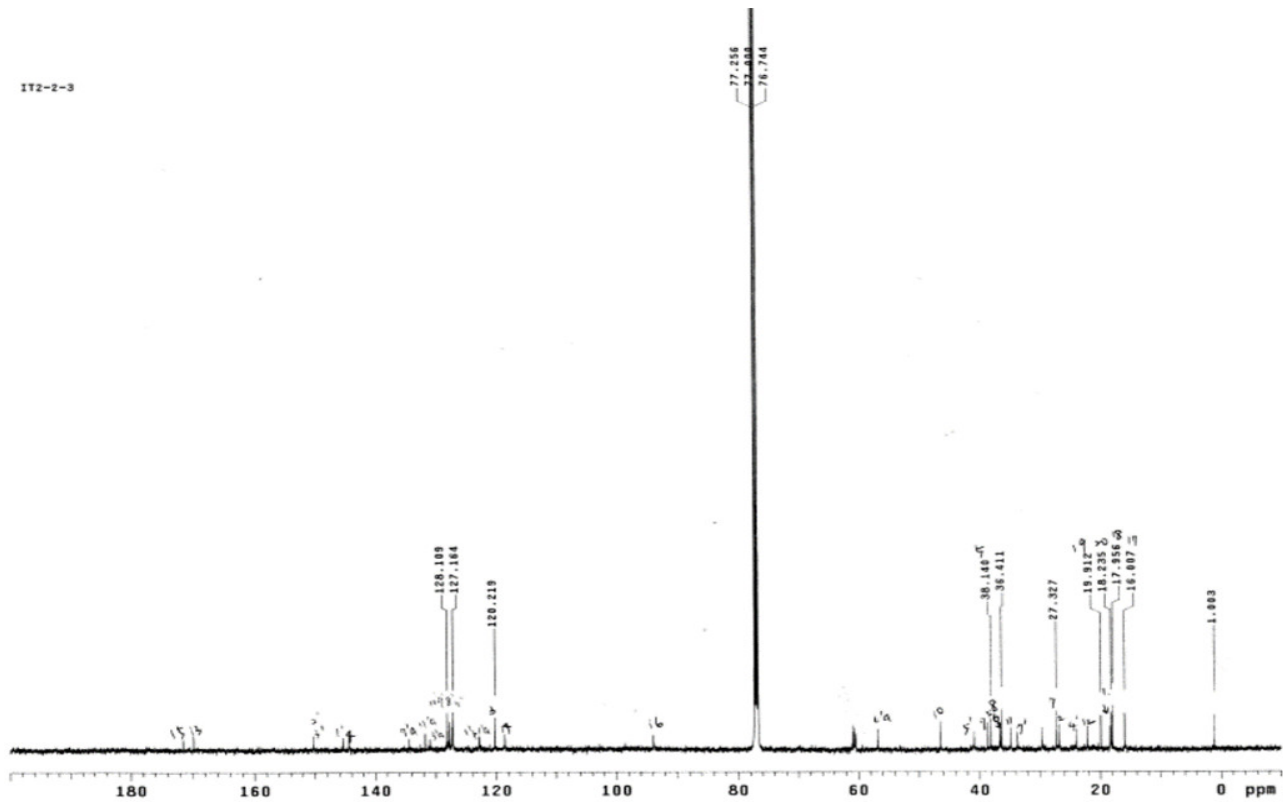
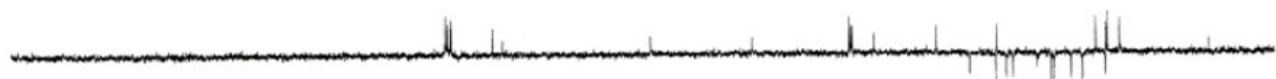


Figure PB-7. ¹³C-NMR spectrum of polyalongarin B (2) in CDCl₃ (125 MHz)

CH/CH₃ up , CH₂ down



CH carbons

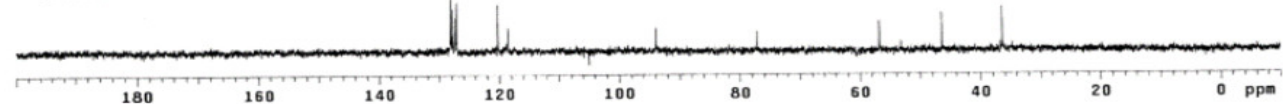


Figure PB-8. DEPT-135 and DEPT-90 spectra of polyalongarin B (2)

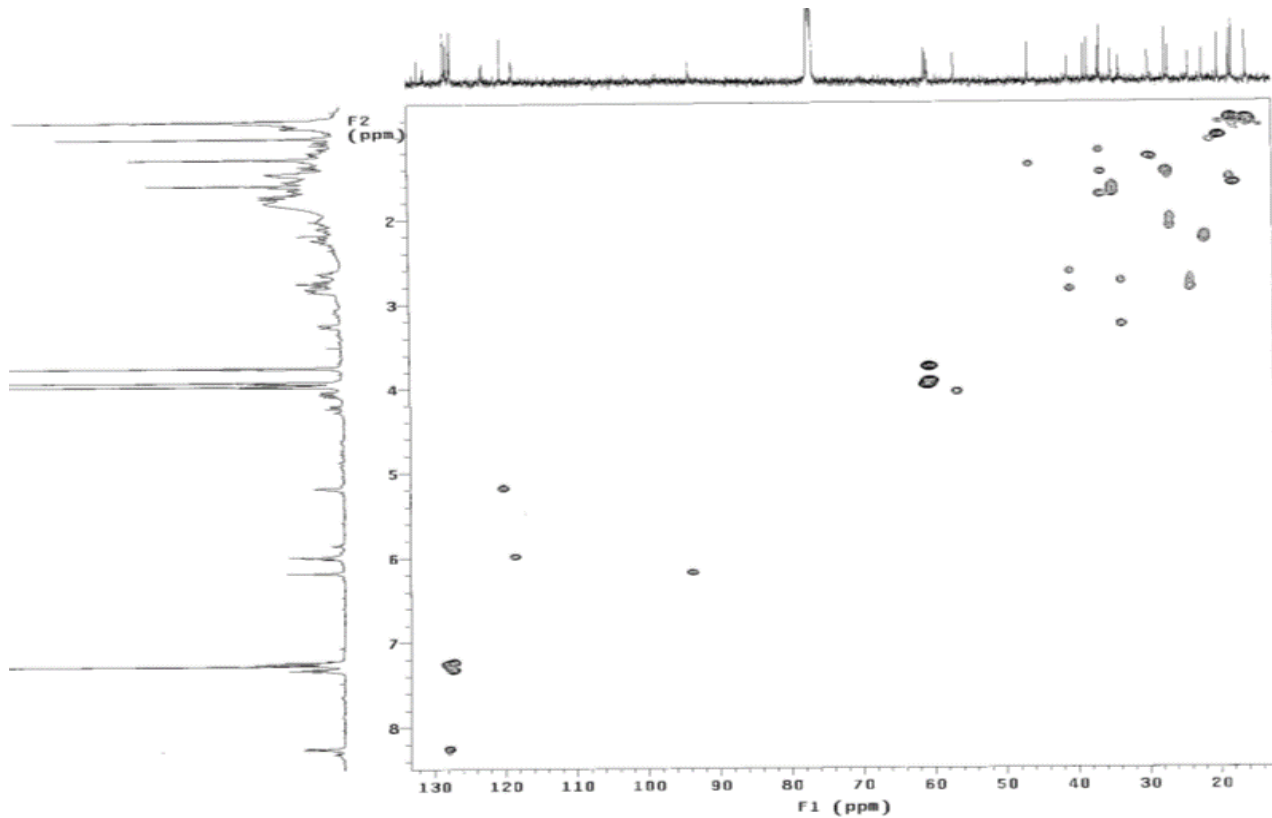


Figure PB-9. HMQC spectrum of polyalongarin B (2)

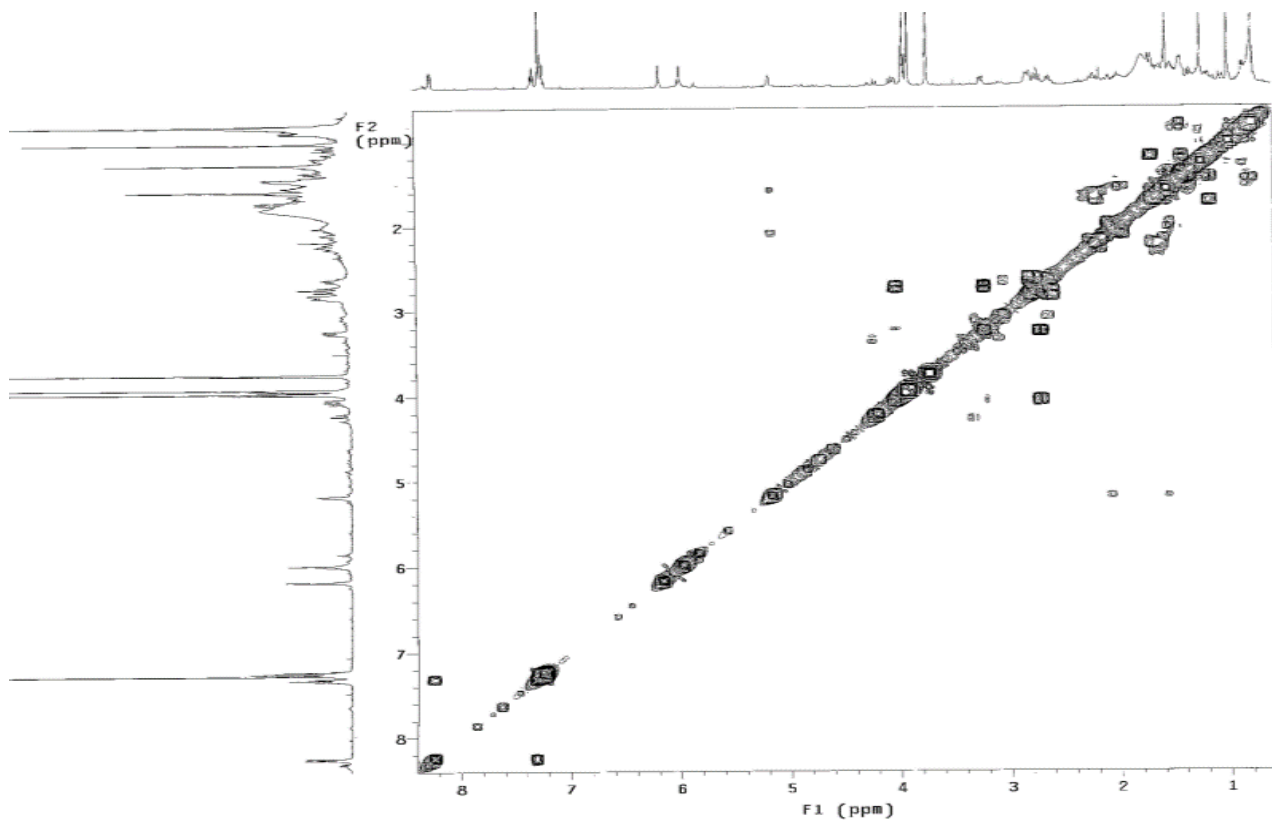


Figure PB-10. COSY spectrum of polyalongarin B (2)

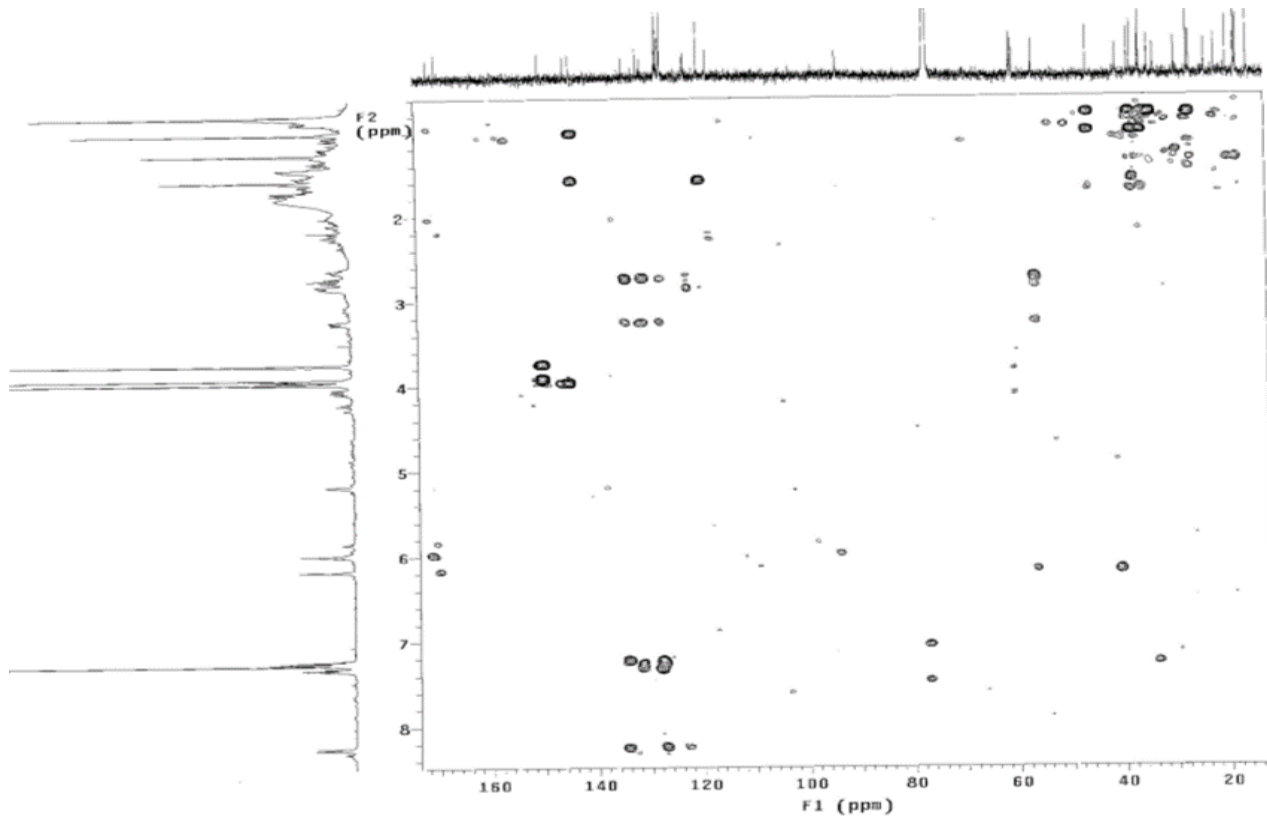


Figure PB-11. HMBC spectrum of polyalongarin B (2)

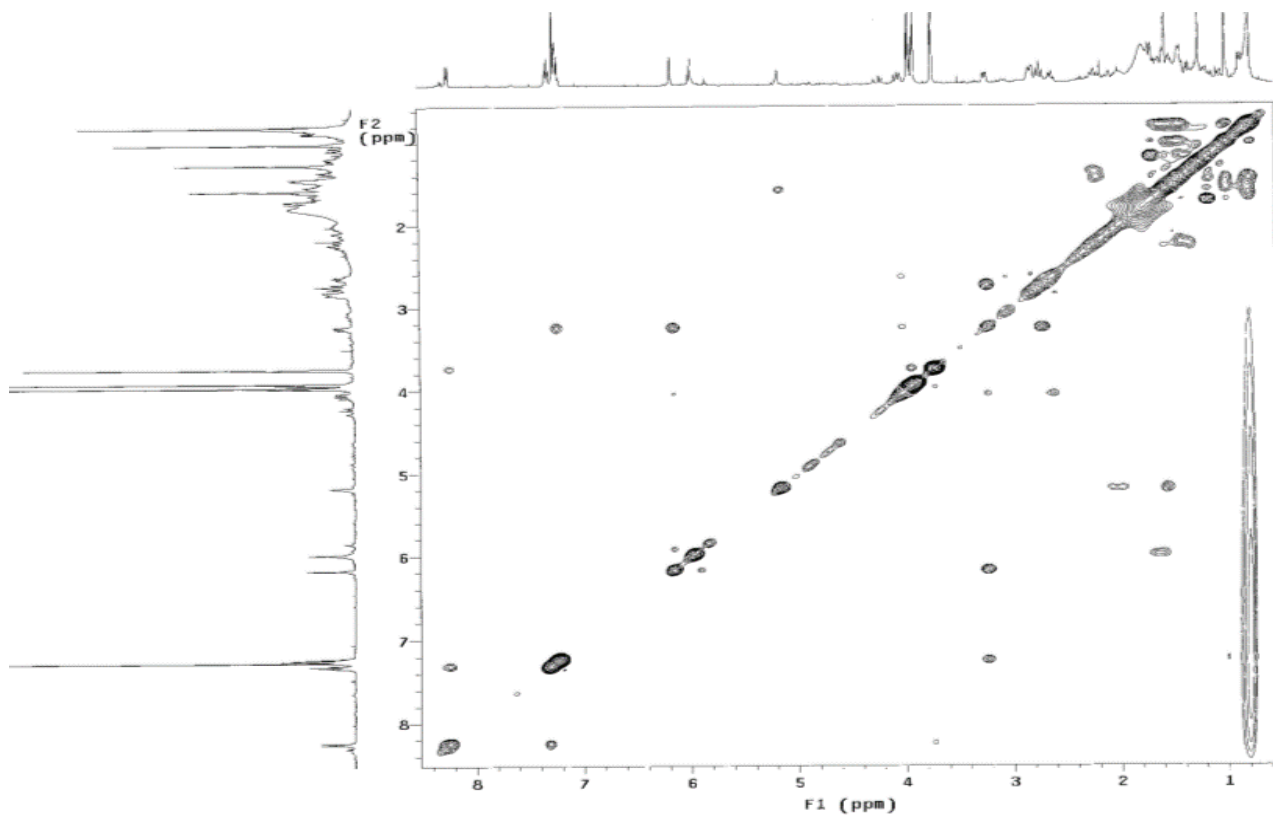
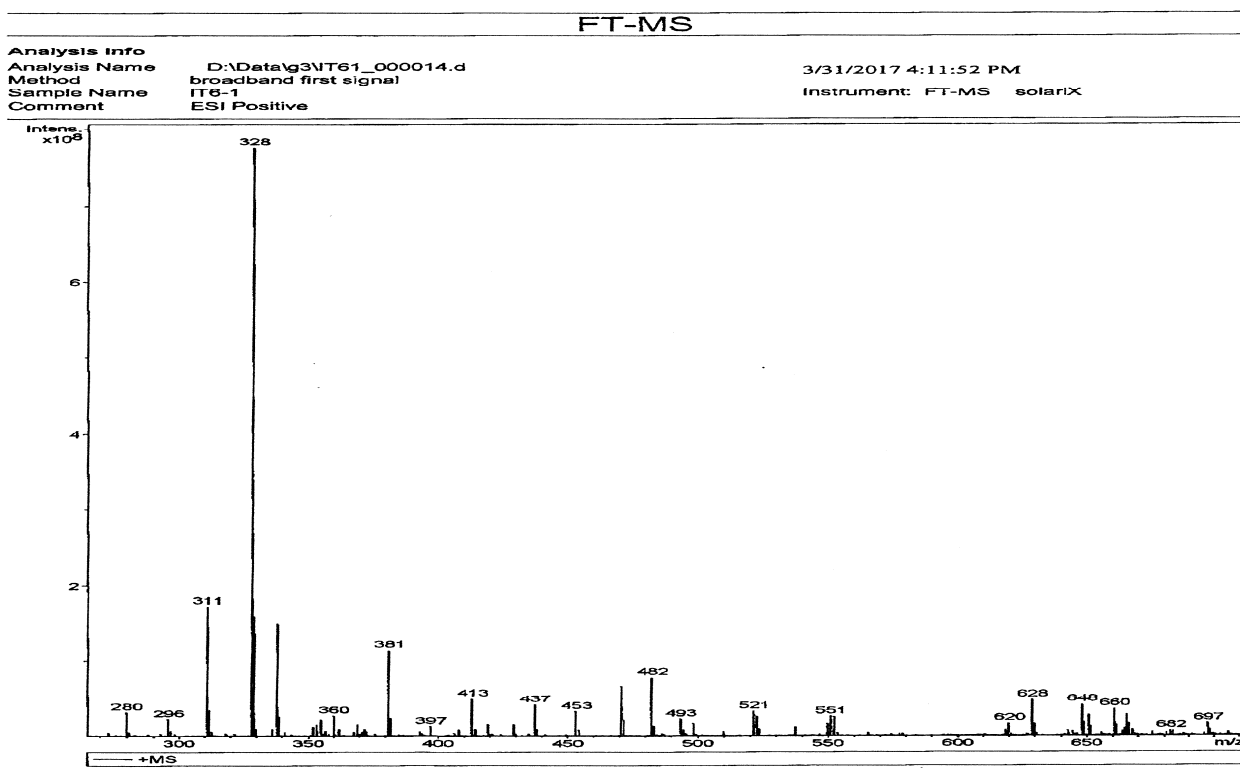
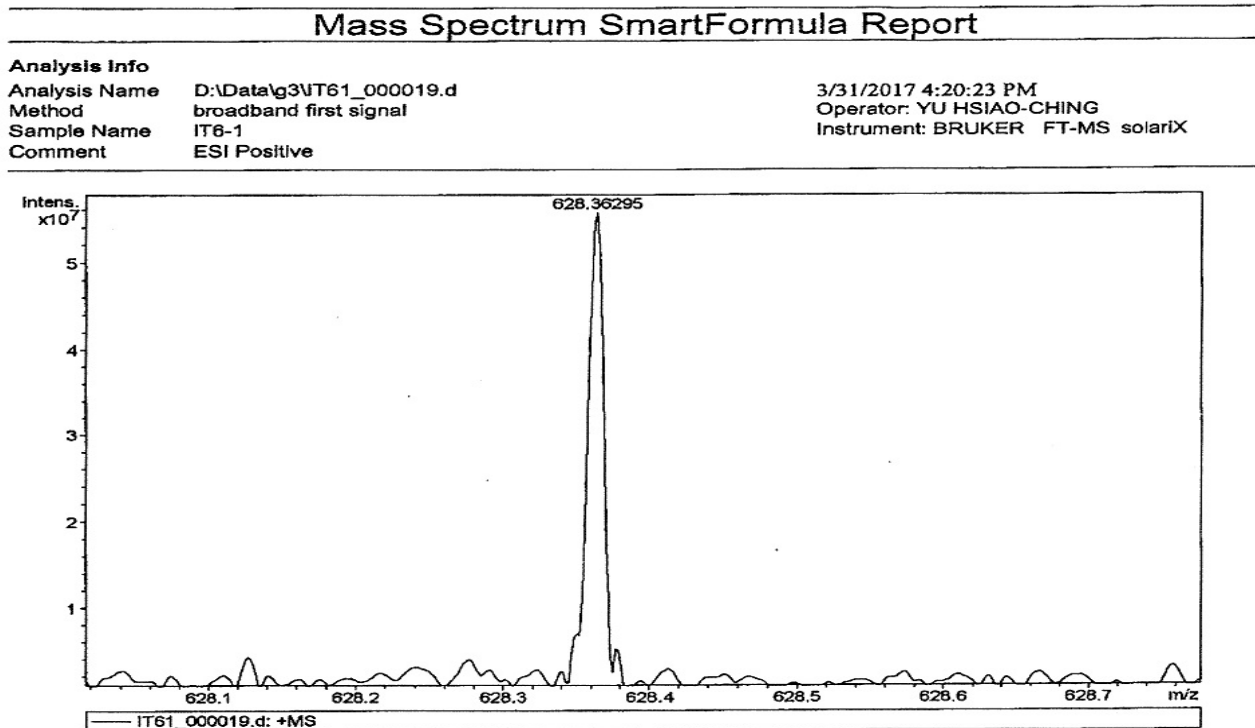


Figure PB-12. NOESY spectrum of polyalongarin B (2)



Bruker Compass DataAnalysis 4.0 printed: 3/31/2017 4:11:52 PM Page 1 of 1

Figure PC-1. ESI-MS spectrum of polyalongarin C (3)



| Meas. m/z | # | Formula | Score | m/z | err [mDa] | err [ppm] | mSigma | rdb | e ⁻ Conf | N-Rule |
|-----------|---|-----------------|--------|-----------|-----------|-----------|--------|------|---------------------|--------|
| 628.36295 | 1 | C 39 H 50 N O 6 | 100.00 | 628.36326 | 0.31 | 0.50 | 54.5 | 15.5 | even | ok |

Figure PC-2. HR-ESI-MS spectrum of polyalongarin C (3)

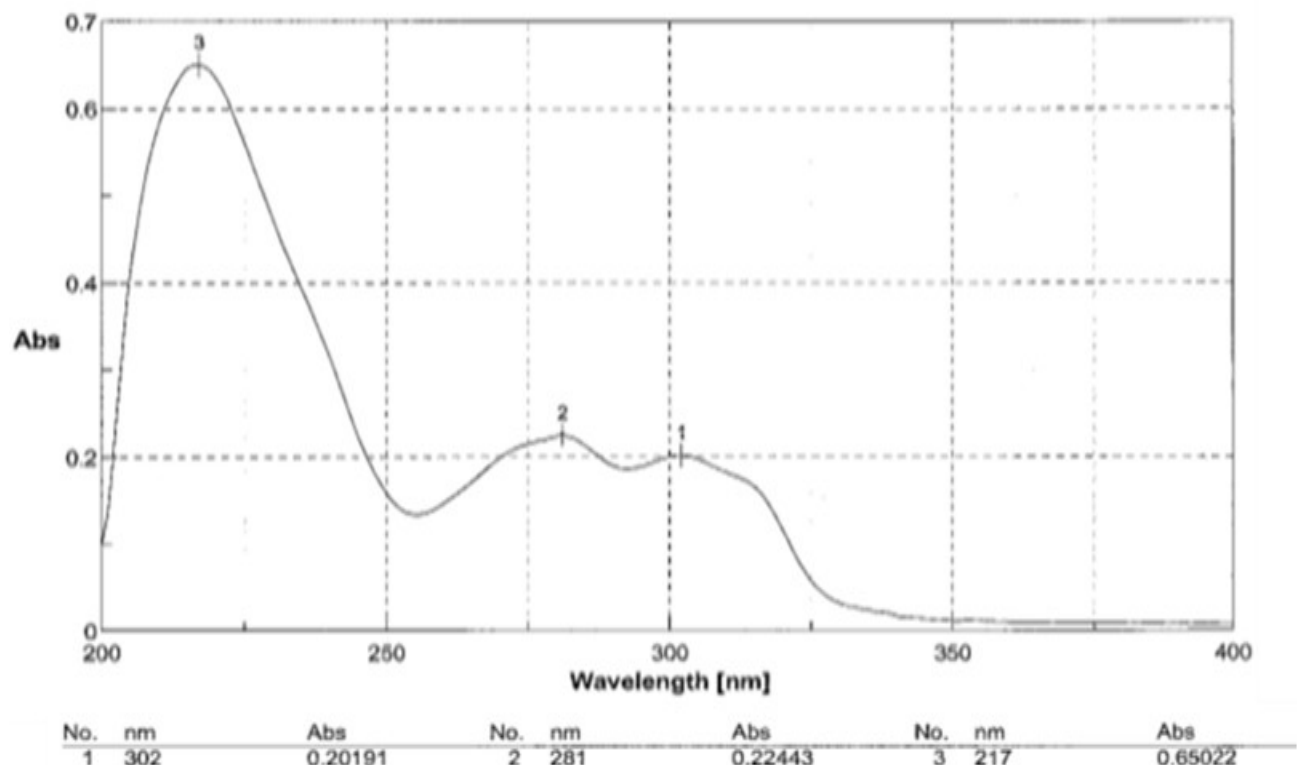
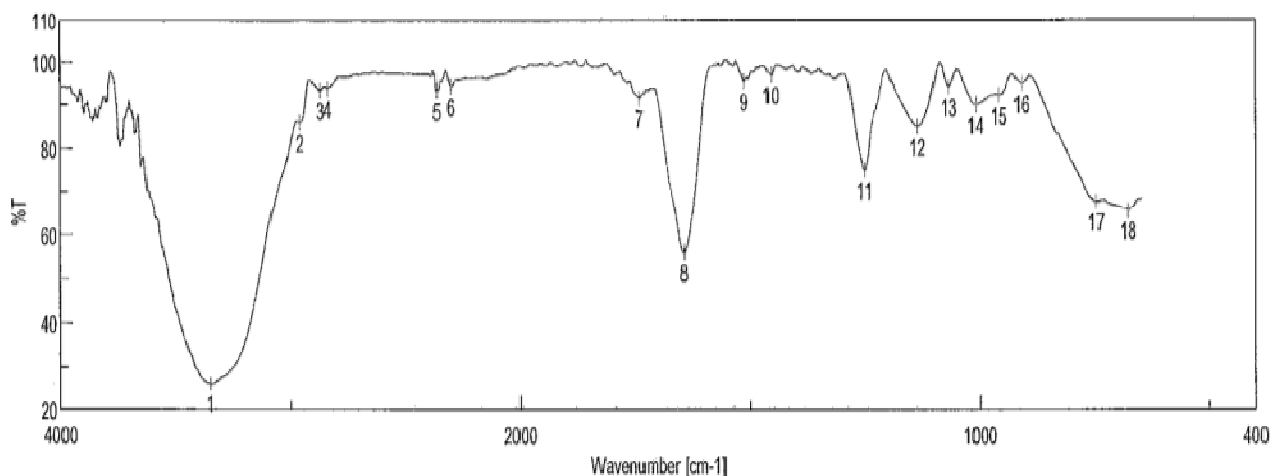


Figure PC-3. UV spectrum of polyalongarin C (3)



[Result of Peak Picking]

| No. | Position | Intensity | No. | Position | Intensity | No. | Position | Intensity |
|-----|----------|-----------|-----|----------|-----------|-----|----------|-----------|
| 1 | 3349.75 | 26.153 | 2 | 2959.23 | 85.9833 | 3 | 2871.49 | 93.3423 |
| 4 | 2838.7 | 93.7338 | 5 | 2362.37 | 93.312 | 6 | 2301.63 | 94.3505 |
| 7 | 1740.44 | 91.7453 | 8 | 1644.02 | 56.1846 | 9 | 1513.85 | 95.6288 |
| 10 | 1454.06 | 97.2024 | 11 | 1251.58 | 75.2242 | 12 | 1135.87 | 85.2725 |
| 13 | 1068.37 | 94.4238 | 14 | 1008.59 | 90.2655 | 15 | 958.448 | 92.4517 |
| 16 | 909.272 | 95.1685 | 17 | 746.317 | 67.8551 | 18 | 675.928 | 65.7945 |

Figure PC-5. IR spectrum of polyalongarin C (3)

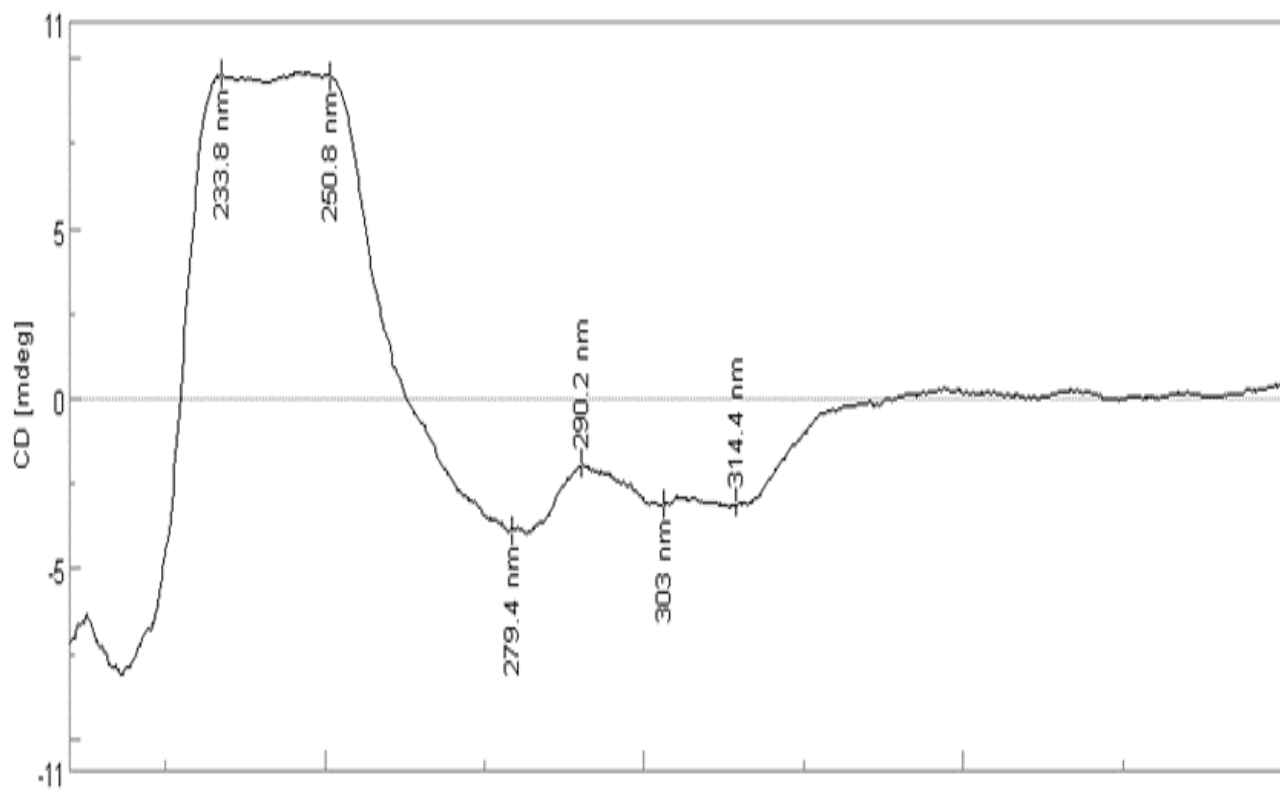


Figure PC-5. CD spectrum of polyalongarin C (3)

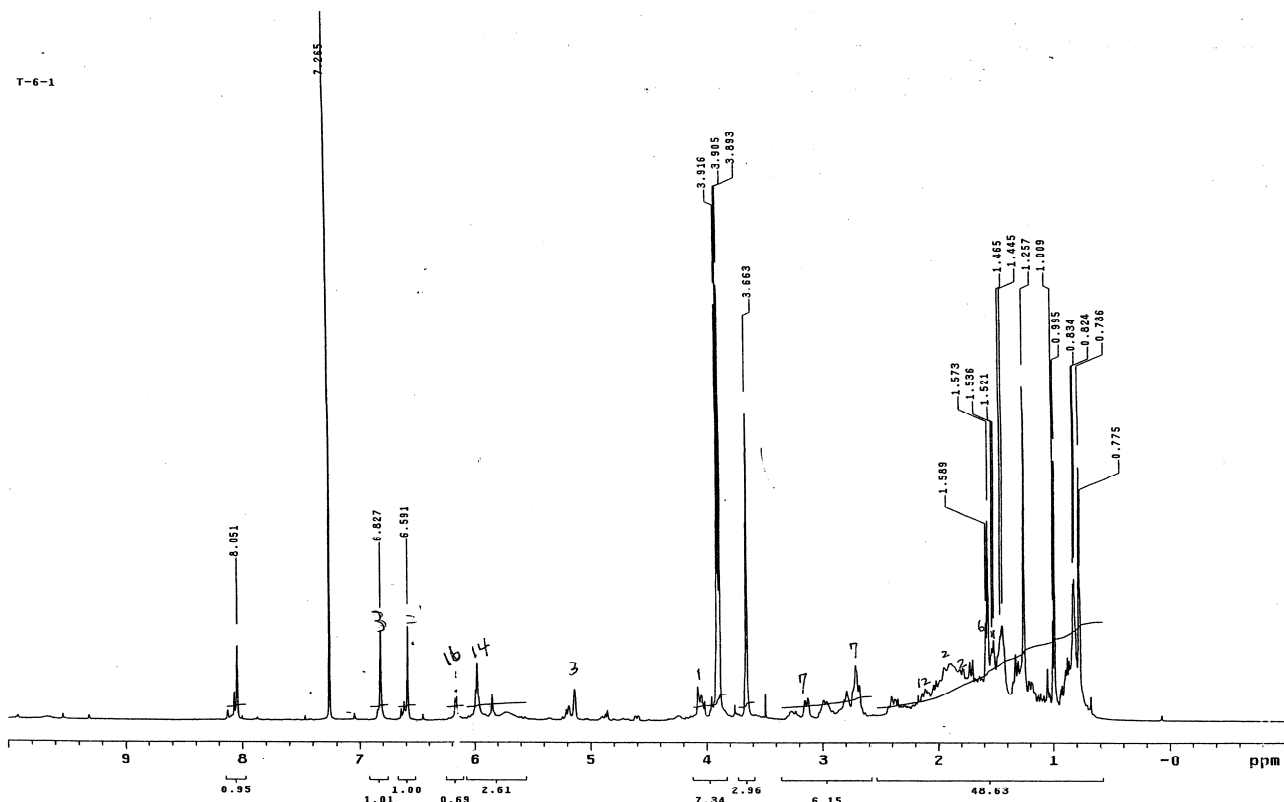


Figure PC-6. ¹H-NMR spectrum of polyalongarin C (3) in CDCl_3 (500 MHz)

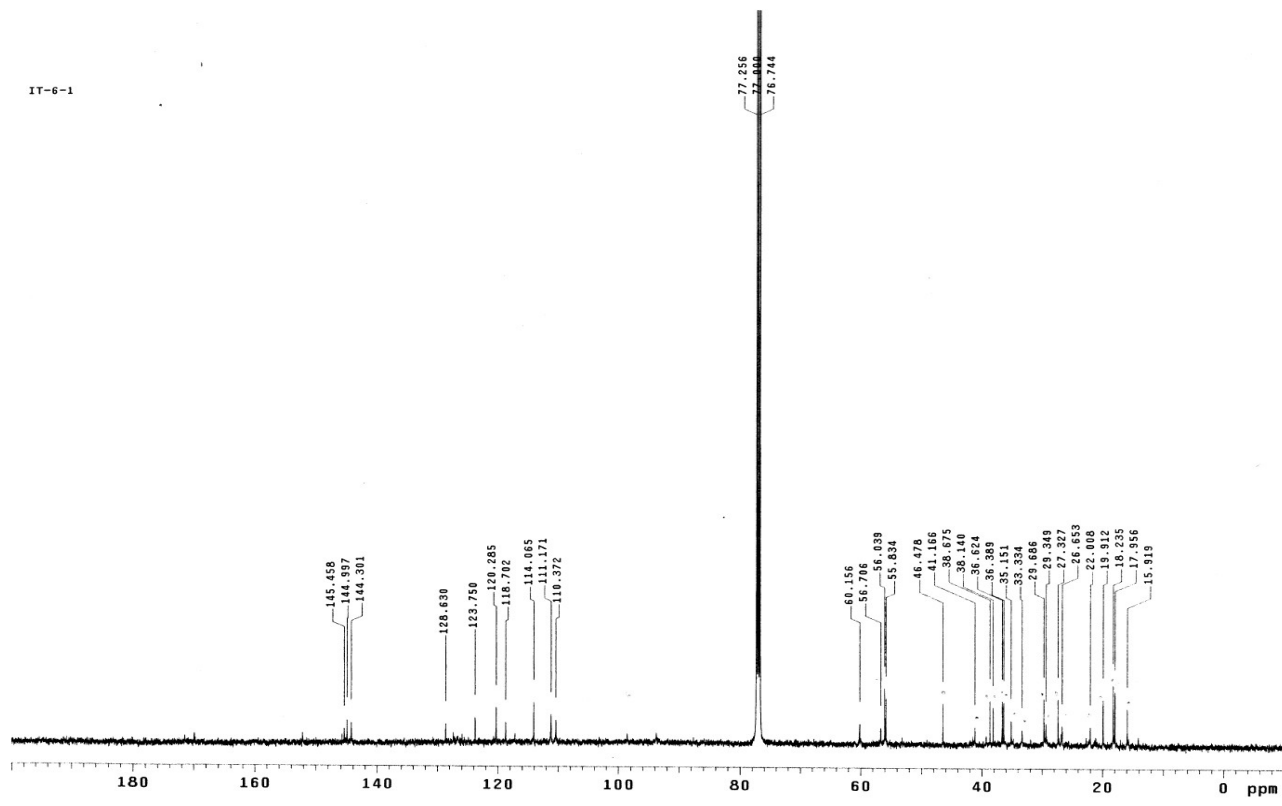


Figure PC-7. ^{13}C -NMR spectrum of polyalongarin C (**3**) in CDCl_3 (125 MHz)

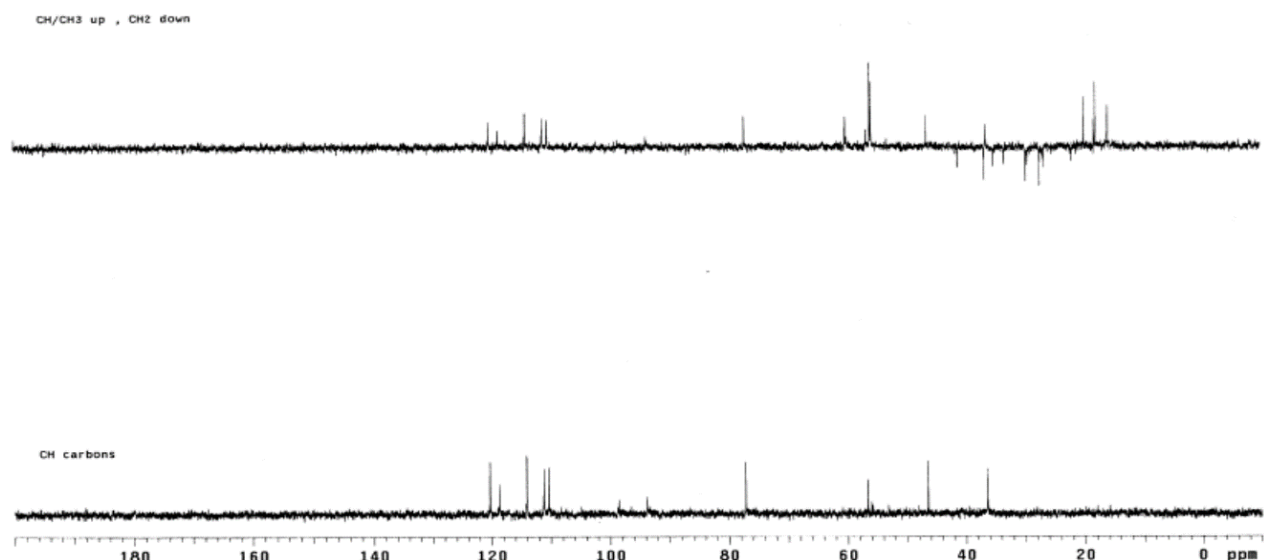


Figure PC-8. DEPT-135 and DEPT-90 spectra of polyalongarin C (**3**)

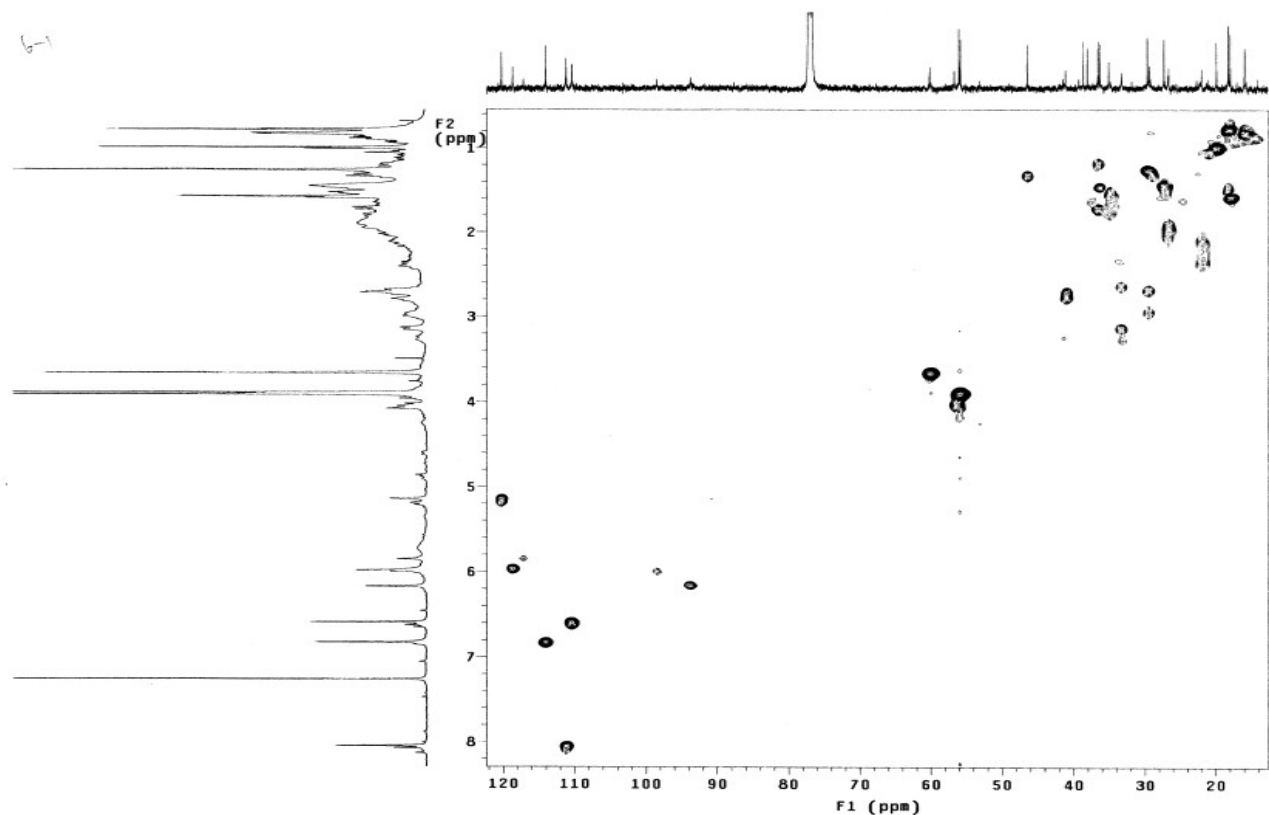


Figure PC-9. HMQC spectrum of polyalongarin C (3)

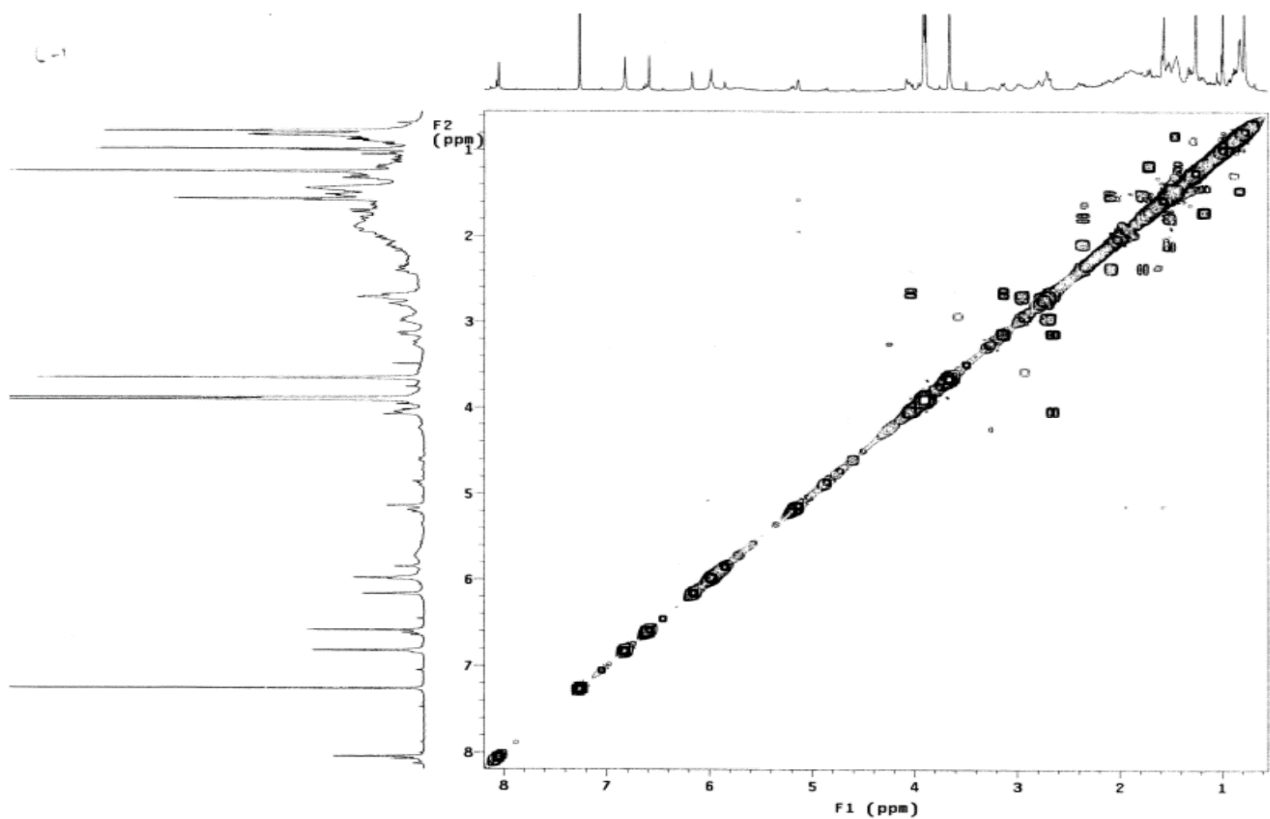


Figure PC-10. COSY spectrum of polyalongarin C (3)

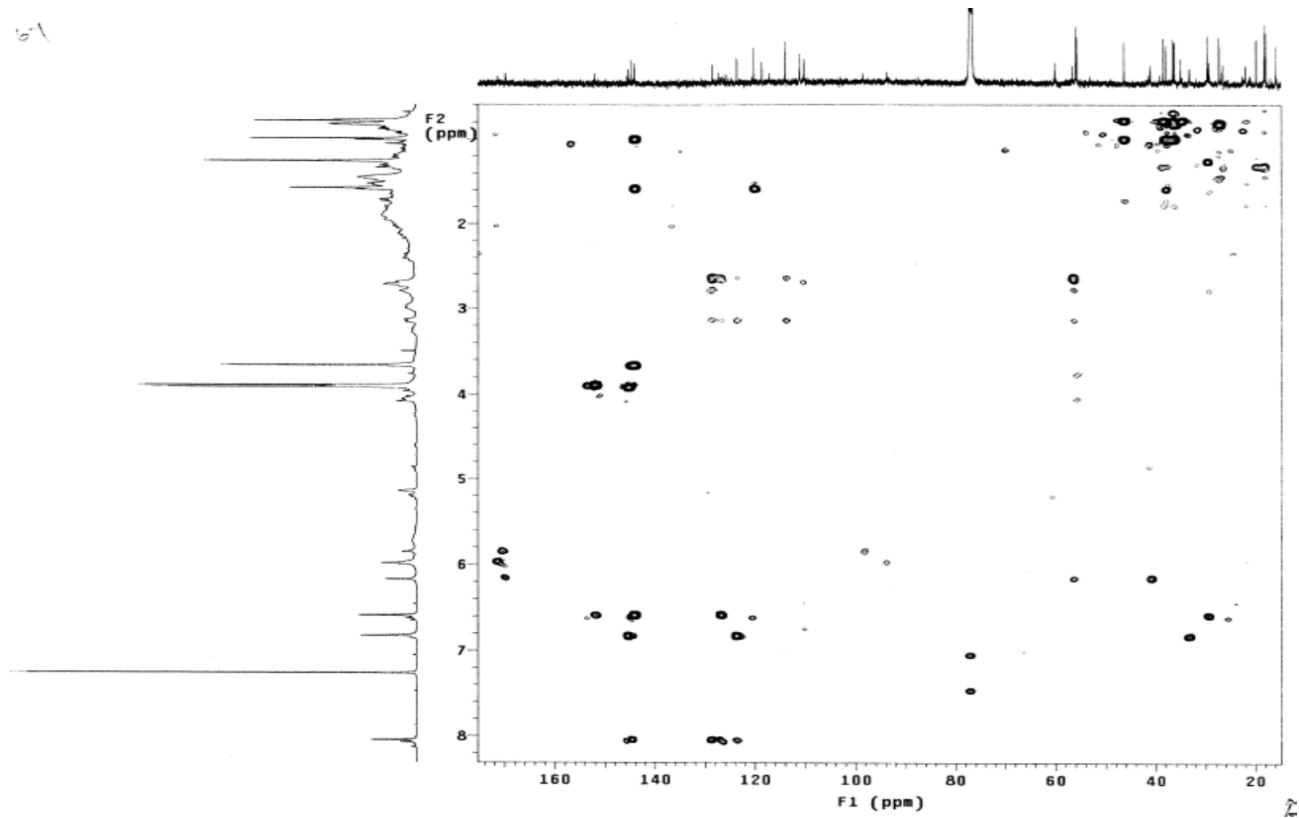


Figure PC-11. HMBC spectrum of polyalongarin C (3)

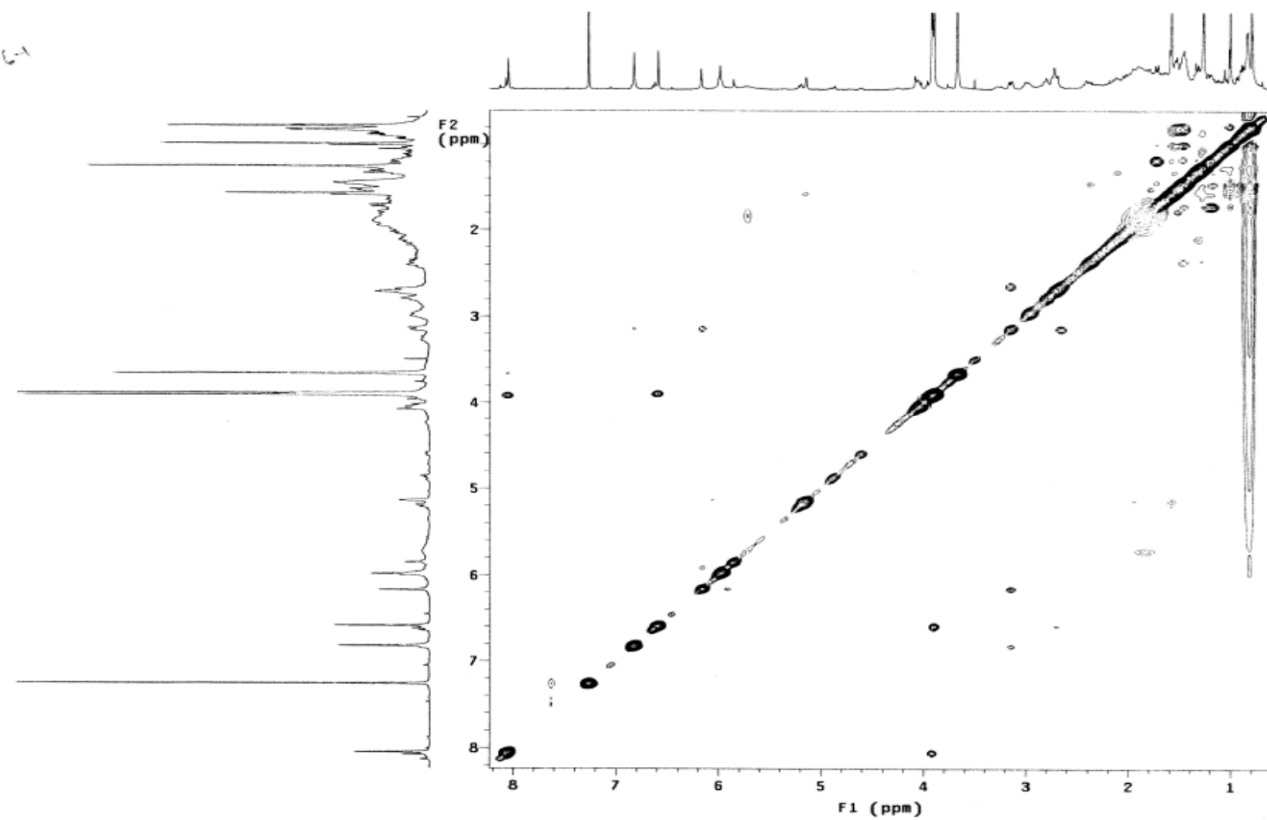


Figure PC-12. NOESY spectrum of polyalongarin C (3)

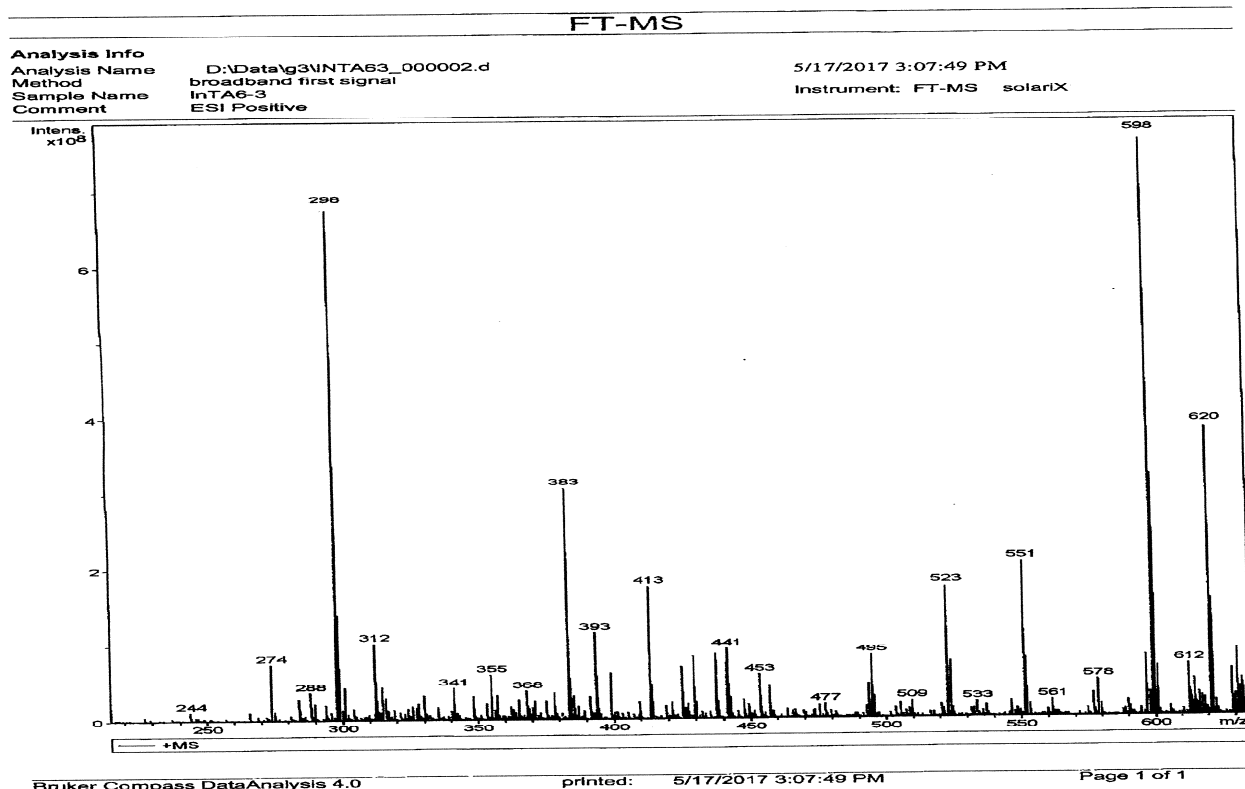
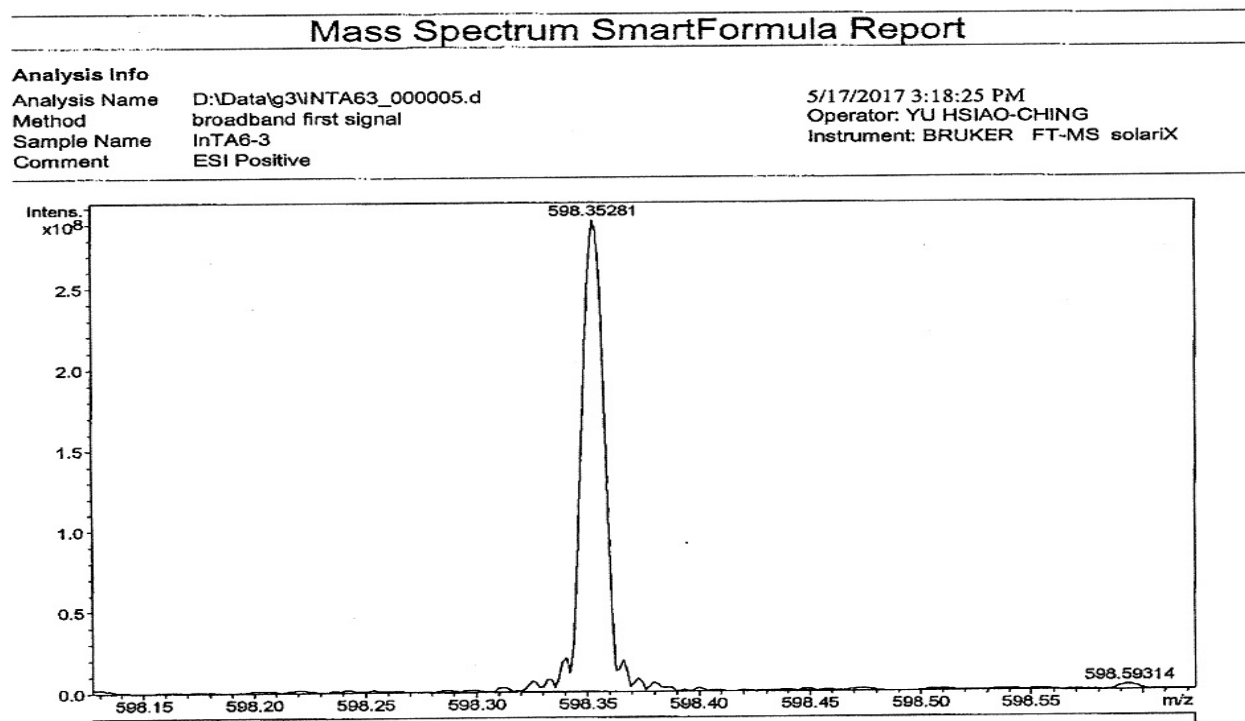


Figure PD-1. ESI-MS spectrum of polyalongarin D (4)



| Meas. m/z | # | Formula | Score | m/z | err [mDa] | err [ppm] | mSigma | rdb | e ⁻ Conf | N-Rule |
|-----------|---|-----------------|--------|-----------|-----------|-----------|--------|------|---------------------|--------|
| 598.35281 | 1 | C 38 H 48 N O 5 | 100.00 | 598.35270 | -0.11 | -0.18 | 3.7 | 15.5 | even | ok |

Figure PD-2. HR-ESI-MS spectrum of polyalongarin D (4)

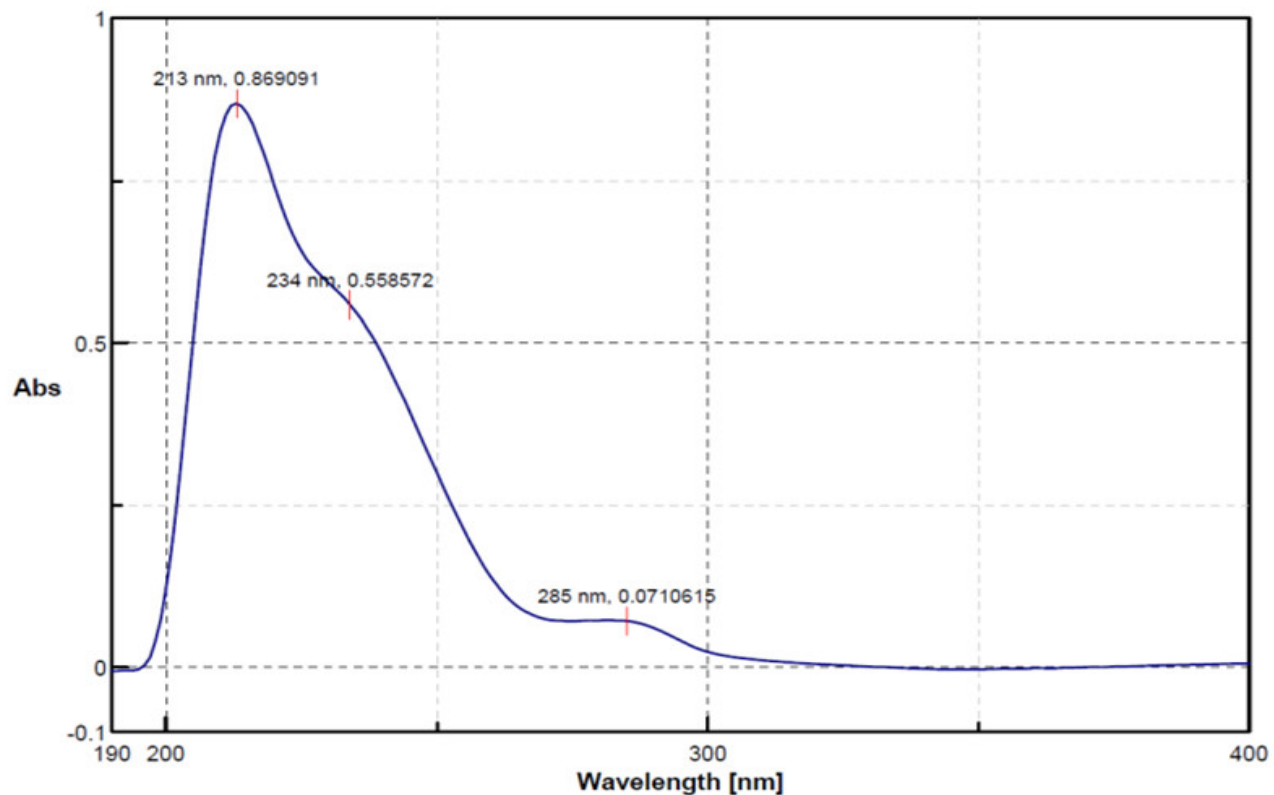
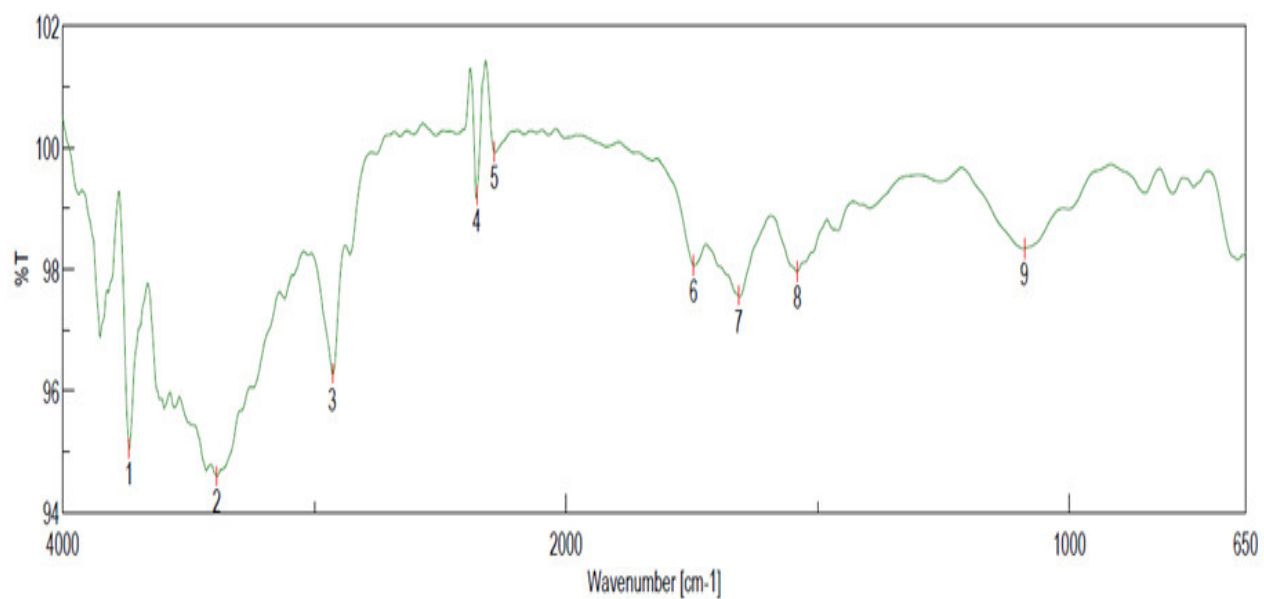


Figure PD-3. UV spectrum of polyalongarin D (4)



[Result of Peak Picking]

| No. | Position | Intensity | No. | Position | Intensity | No. | Position | Intensity |
|-----|----------|-----------|-----|----------|-----------|-----|----------|-----------|
| 1 | 3736.4 | 95.0491 | 2 | 3388.32 | 94.5968 | 3 | 2929.34 | 96.2745 |
| 4 | 2355.62 | 99.205 | 5 | 2285.23 | 99.9143 | 6 | 1747.19 | 98.0573 |
| 7 | 1657.52 | 97.5618 | 8 | 1540.85 | 97.9485 | 9 | 1089.58 | 98.337 |

Figure PD-4. IR spectrum of polyalongarin D (4)

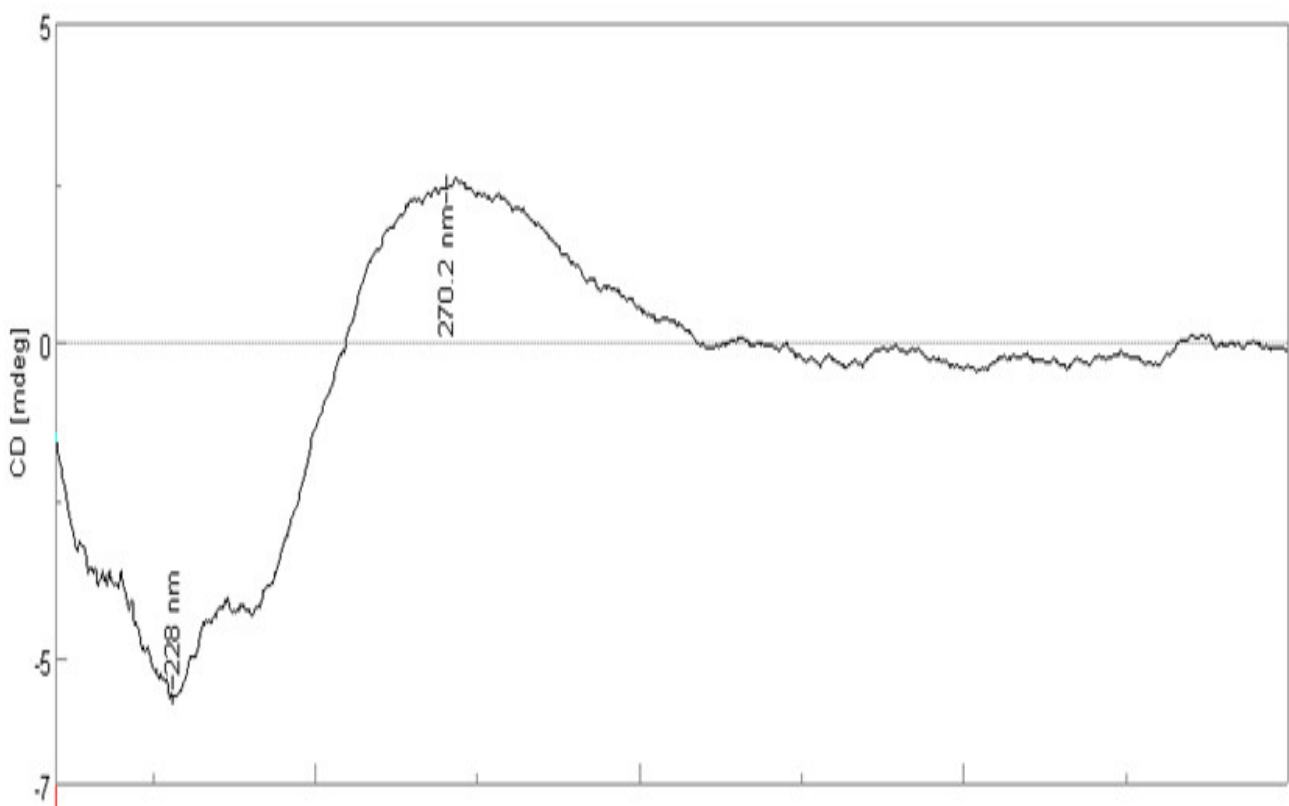


Figure PD-5. CD spectrum of polyalongarin D (**4**)

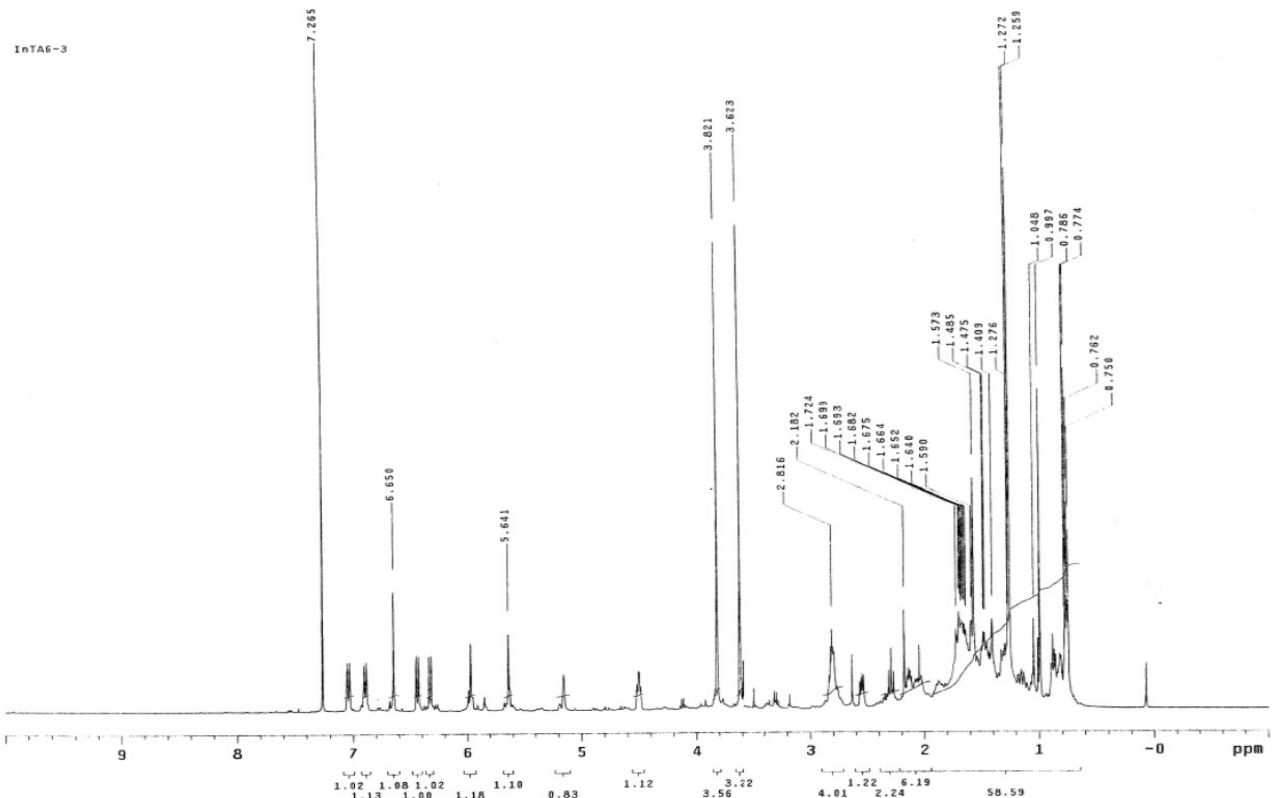


Figure PD-6. ^1H -NMR spectrum of polyalalongarin D (**4**) in CDCl_3 (500 MHz)

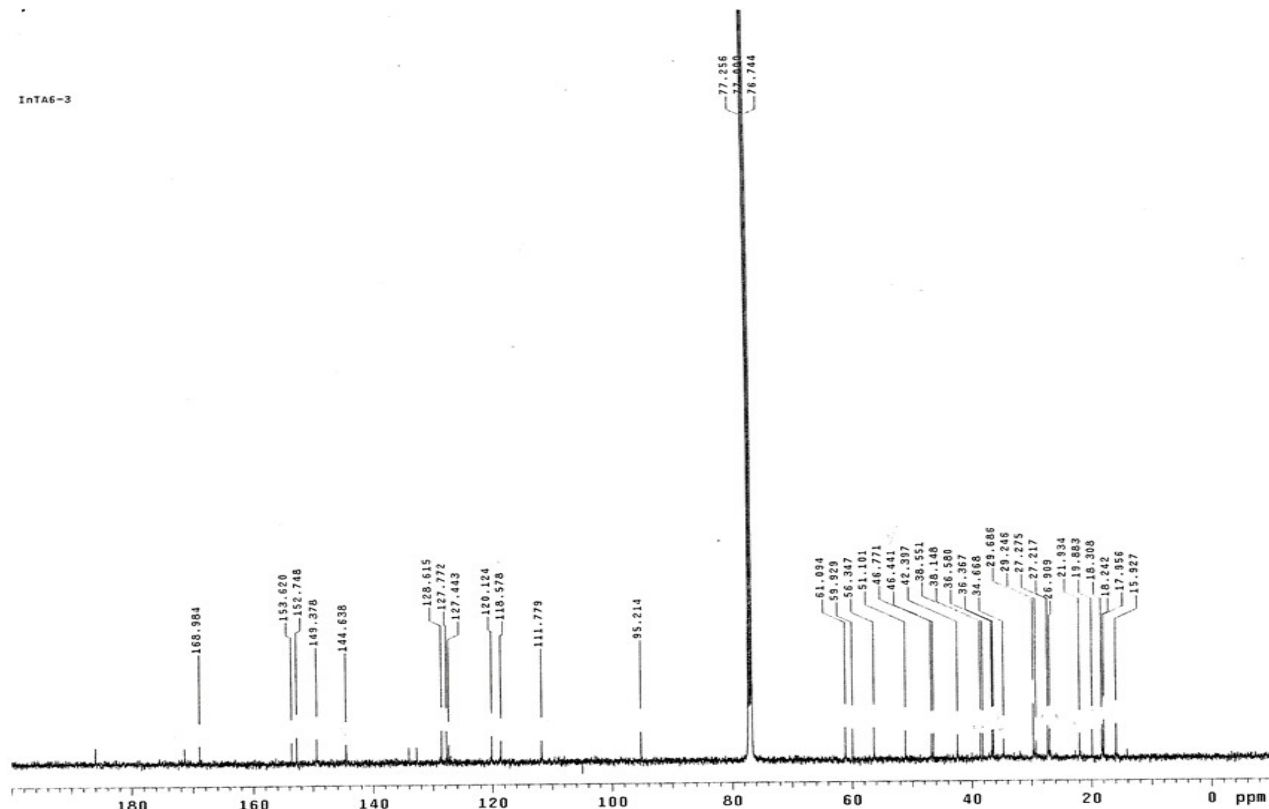


Figure PD-7. ^{13}C -NMR spectrum of polyalongarin D (4) in CDCl_3 (125 MHz)

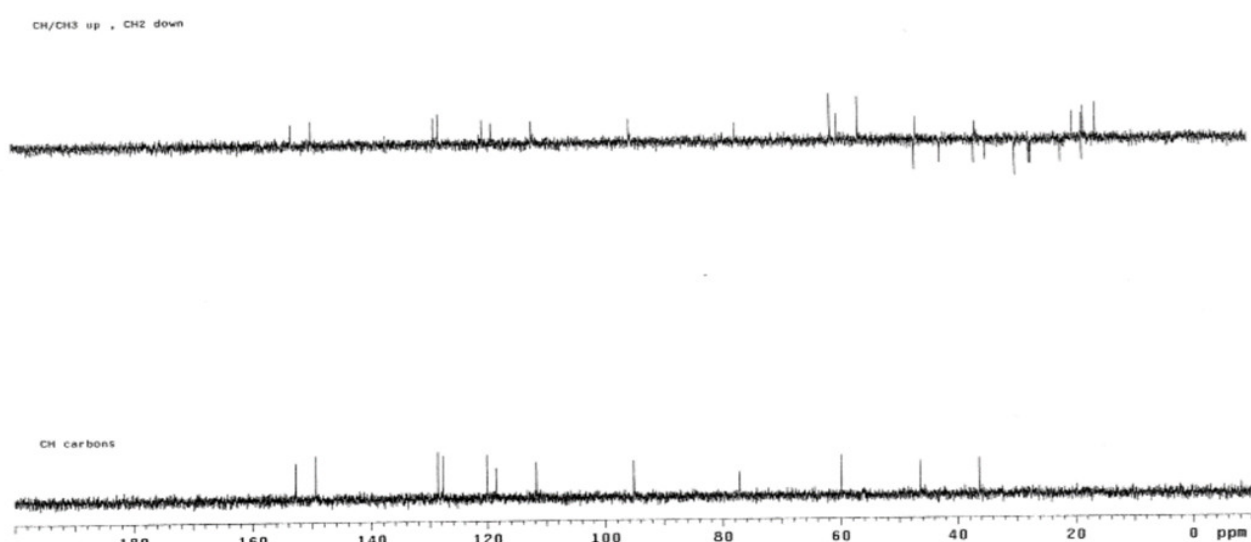


Figure PD-8. DEPT-135 and DEPT-90 spectra of polyalongarin D (4)

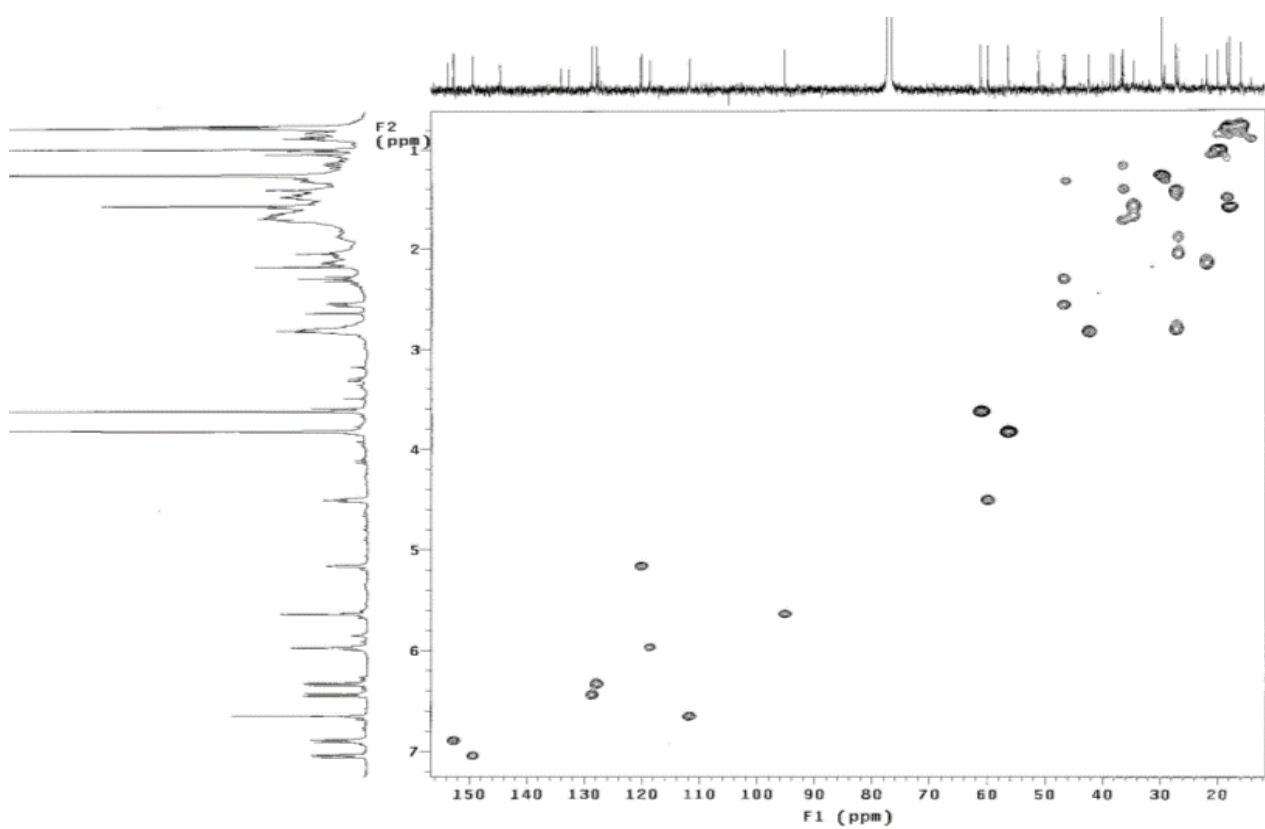


Figure PD-9. HMQC spectrum of polyalongarin D (4)

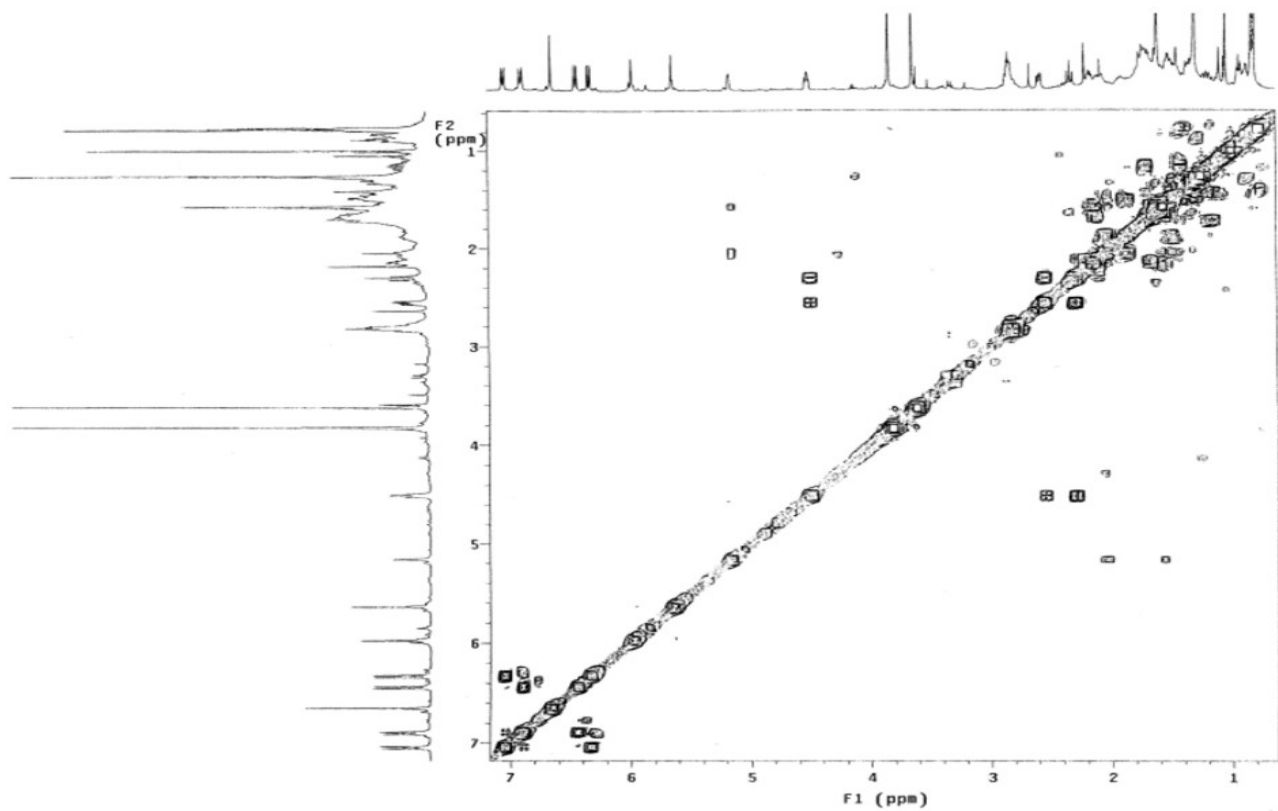


Figure PD-10. COSY spectrum of polyalongarin D (4)

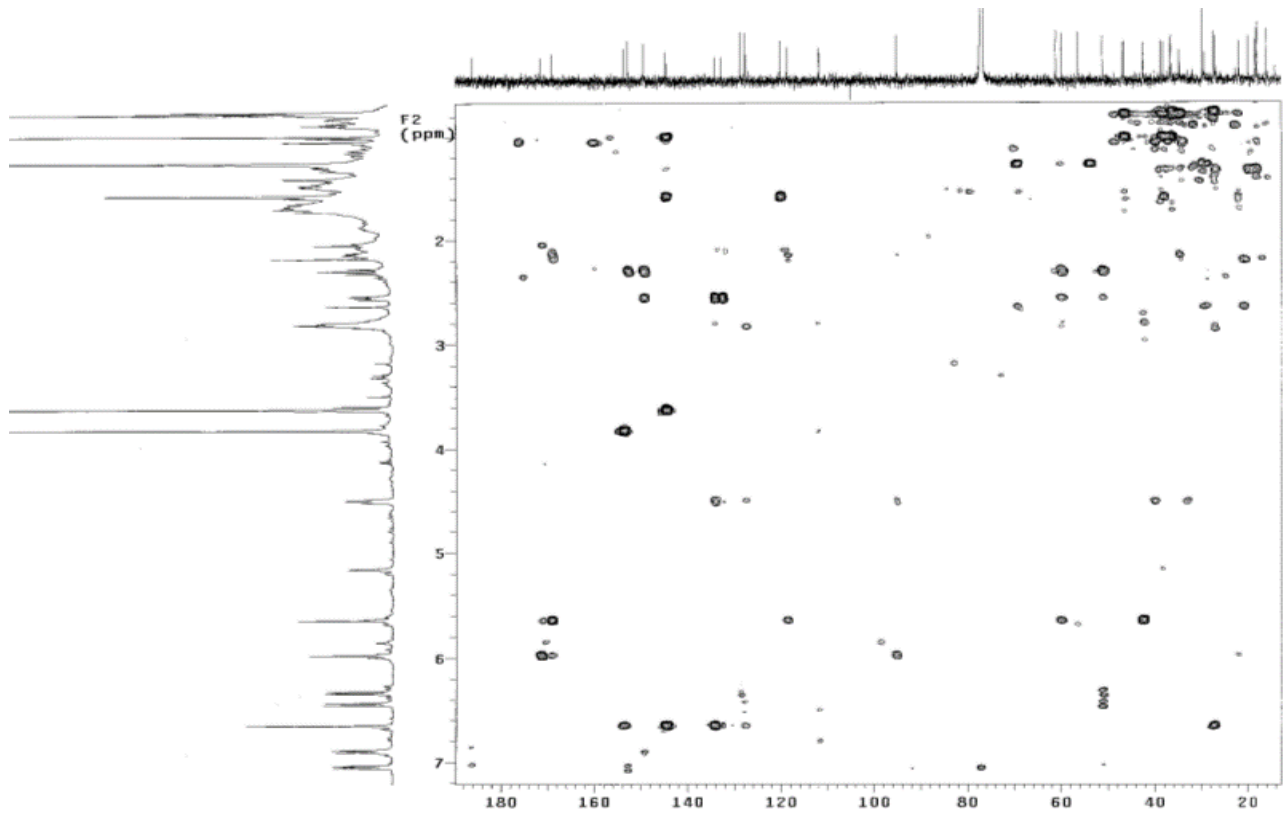


Figure PD-11. HMBC spectrum of polyalongarin D (4)

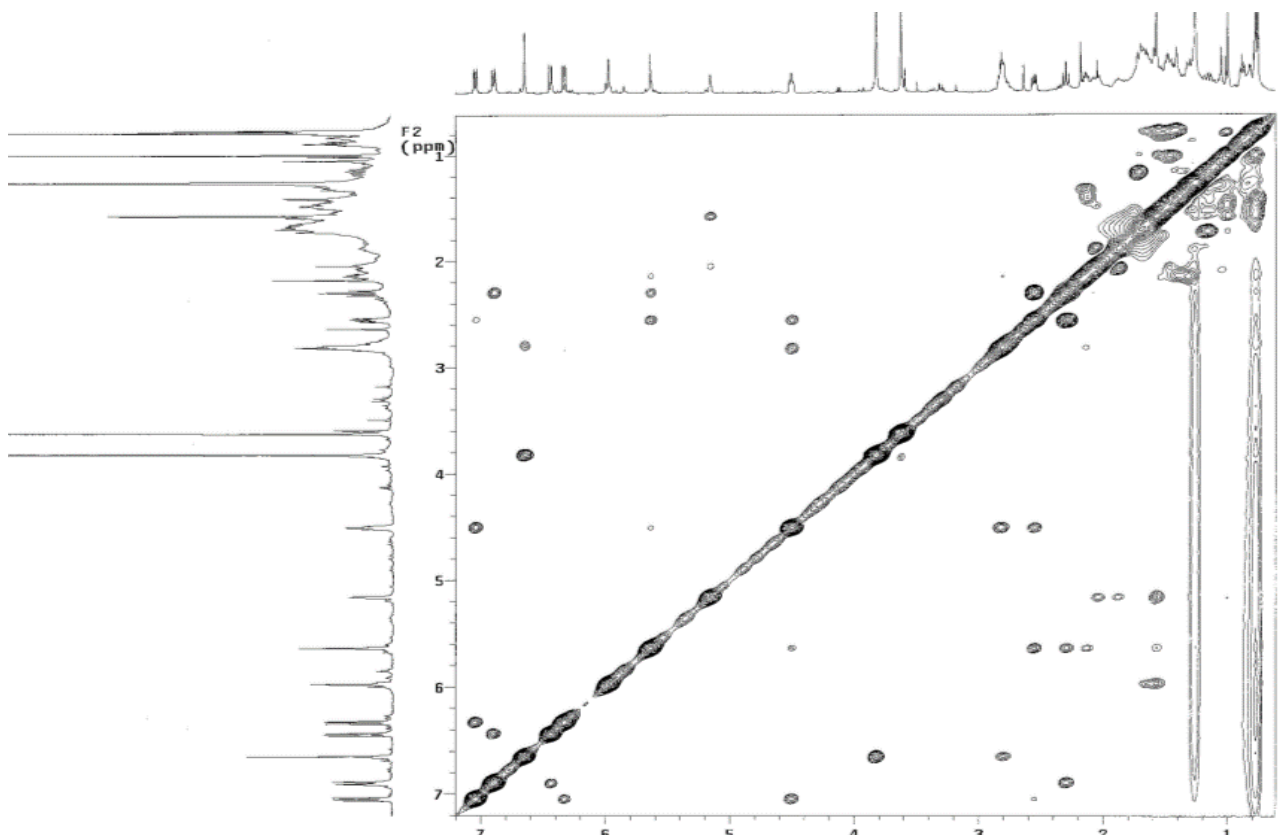


Figure PD-12. NOESY spectrum of polyalongarin D (4)